Journal Pre-proof

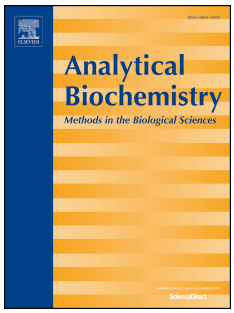

Characterization of Biomolecular Interactions by Biophysical Methods.

Aysha K. Demeler, James Bosco, Matthew J. Sydor, Michelle Nemetchek, Saeed Mortezazadeh, Liam Kerr, Sophia Bird, Roza Gabdullina, Cindee Yates-Hansen, Levi J. McClelland, Ekaterina Voronina, Trushar R. Patel, Borries Demeler

PII: S0003-2697(25)00097-1

DOI: https://doi.org/10.1016/j.ab.2025.115859

Reference: YABIO 115859

To appear in: *Analytical Biochemistry*

Received Date: 16 January 2025

Revised Date: 13 March 2025

Accepted Date: 31 March 2025

Please cite this article as: A.K. Demeler, J. Bosco, M.J. Sydor, M. Nemetchek, S. Mortezazadeh, L. Kerr, S. Bird, R. Gabdullina, C. Yates-Hansen, L.J. McClelland, E. Voronina, T.R. Patel, B. Demeler, Characterization of Biomolecular Interactions by Biophysical Methods., *Analytical Biochemistry*, https://doi.org/10.1016/j.ab.2025.115859.

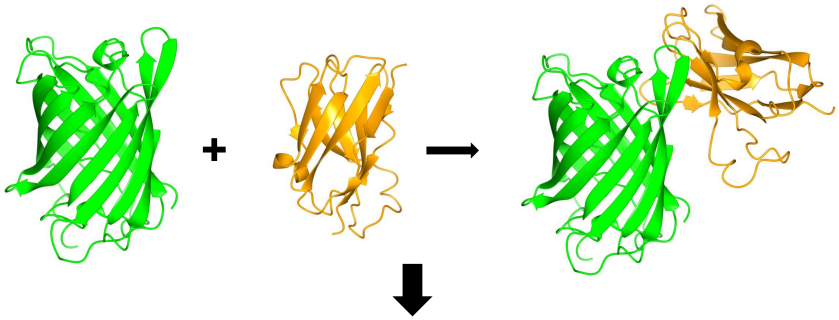

ITC

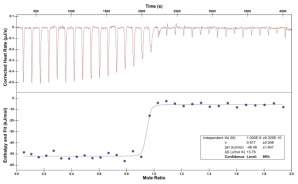

MW-AUC

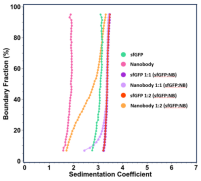

F-AUC

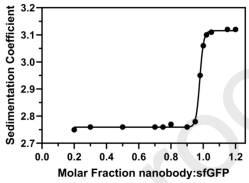

MST

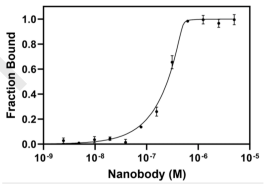

FCS

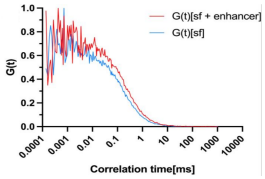

SEC-MALS

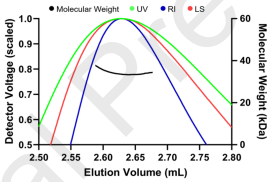

SEC-DLS

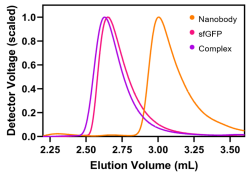

$\bar{\nu}$Title

Characterization of Biomolecular Interactions by Biophysical Methods.

Authors

Aysha K. Demeler[1*)], James Bosco[2*)], Matthew J. Sydor[2,3], Michelle Nemetchek[2,3], Saeed Mortezazadeh[1], Liam Kerr[1], Sophia Bird[1], Roza Gabdullina[1], Cindee Yates-Hansen[3], Levi J. McClelland[2,3], Ekaterina Voronina[3], Trushar R. Patel[1], Borries Demeler[1,2**)]

*) Equal contribution

**) Corresponding Author

1. Department of Chemistry and Biochemistry, University of Lethbridge, Lethbridge, AB, T1K 3M4, Canada

2. Department of Chemistry and Biochemistry, University of Montana, Missoula, MT 59812, USA

3. Division of Biological Sciences, University of Montana, Missoula, MT 59812, USA

4. Center for Biomolecular Structure & Dynamics, University of Montana, Missoula, MT 59812, USA

In memory of our dear friend and mentor Alexander ("Sandy") Ross who taught us fluorescence spectroscopy.

Abstract

This study compares several analytical biophysical methods for investigating protein-protein interactions (PPIs) in solution, using the interaction between superfolder green fluorescent protein (sfGFP) and its anti-sfGFP nanobody enhancer as a model system. Techniques evaluated include microscale thermophoresis, fluorescence correlation spectroscopy, analytical ultracentrifugation with multi-wavelength and fluorescence detection, isothermal titration calorimetry, and analytical size exclusion chromatography coupled to multi-angle static light scattering and dynamic light scattering. Each method was assessed for information content, dynamic range, precision, and complementarity. The results consistently indicate a single-digit nanomolar dissociation constant and 1:1 stoichiometry for the interaction. While each technique offers unique insights into binding affinity, thermodynamics, and stoichiometry of the interaction, the multi-method approach provides a more complete and reliable characterization of PPIs. The study demonstrates how combining multiple complementary techniques enhances the robustness of PPI analysis in solution-phase conditions.

Introduction

Macromolecular interactions between biomolecules (proteins, DNA, RNA, lipids, carbohydrates) are of central interest to studying processes inside of cells and the molecular basis for disease. Investigators are able to choose from a range of biophysical methods to elucidate the thermodynamic and hydrodynamic properties of reversible protein-protein interactions in order to analyze the structural and functional interactions involved. In this work, we compare and contrast commonly used methods that can be applied in a true solution environment where no binding partners have to be attached to a solid support. We evaluate the strengths and weaknesses of each method and identify the properties that can be measured by each method. For our comparison, we used the same protein-protein interaction model system. Methods include microscale thermophoresis (MST), isothermal titration calorimetry (ITC), analytical ultracentrifugation by multi-wavelength (MW-AUC) and fluorescence detection (F-AUC), size exclusion chromatography, coupled to multi-angle light scattering (SEC-MALS) or dynamic light scattering (DLS), and fluorescence correlation spectroscopy (FCS).

Scientific questions often require the use of diverse techniques, as each method offers unique insights, sensitivities, and capabilities. To obtain a comprehensive understanding of the interaction between two interacting molecules, multiple biophysical methods should be utilized. By systematically applying complementary approaches, a global picture emerges and the precision and confidence in the results increases. This multi-method strategy not only enhances the robustness of the data but also allows cross-validation of our findings, and addresses different aspects of the binding mechanism, from affinity to stoichiometry, oligomerization state, and structural stability. We illustrate the pros and cons of each technique, providing a critical assessment of how these methods complement each other and contribute to a deeper understanding of the interaction. Through this integrative approach, we aim to generate high-confidence results while being mindful of the inherent constraints of each method.

For our comparison, we characterize the interaction between anti-green fluorescent protein (GFP) enhancer nanobodies and superfolder GFP (sfGFP). GFP-enhancer nanobody (nanobody) was originally identified based on its ability to enhance the fluorescence of wild-type GFP [1]. This effect is likely due to stabilization of the anionic state of the chromophore, which was associated with significant modulation of GFP absorption spectrum between 350 and 500 nm, observed for both wild-type GFP and enhanced GFP upon nanobody binding [1].

The same system is employed in each method, so the results can be directly compared between all methods. Anti-GFP nanobodies have been engineered for high specificity and affinity towards GFP and its variants, making them an ideal candidate for microscopy and affinity protein purification. The use of GFP and its variants in molecular and cellular biology has become ubiquitous due to its fluorescence properties, which allows for real-time visualization of biological processes without the need for additional cofactors [2, 3, 4]. GFP is extensively used as a fluorescent tag fused to proteins to study localization and visualize dynamic cellular events *in vitro* and *in vivo* and can also be used for monitoring gene expression through GFP gene fusions [2, 4]. GFP can be fused to proteins without altering the fusion protein's function, however, common issues such as GFP misfolding and aggregation during expression in *E. coli*, often exacerbated by the proteins to which GFP is fused, can arise [5]. To address these challenges, several variants and mutants of GFP have been engineered to enhance the characteristics of the wild-type protein, including improved folding efficiency, photostability, increased fluorescent yield, and a wide range of excitation and emission properties [6, 7]. These enhancements ensure better performance across a range of biological conditions. Proteins fused to superfolder GFP (sfGFP) exhibit superior folding properties and stability, maintaining high fluorescence yield making it particularly suitable for fusion protein applications [5]. In recent years, anti-GFP nanobodies, specifically the GFP-enhancer nanobody, have been engineered as high-affinity binding partners to GFP and its variants for the purpose of purifying GFP-fused proteins of interest [2, 8, 9]. GFP is often fused to human proteins,

which are notoriously challenging to express and purify due to issues such as degradation and formation of insoluble aggregates [8]. By using anti-GFP-nanobodies for affinity purification, researchers can achieve a dual-benefit approach: enhancing the yield and purity of these proteins while preserving the fluorescent properties of GFP for subsequent visualization and analysis. In addition to comparing the utility of the included biophysical methods, we aim to further validate the stability and efficiency of this tool in biotechnology applications. By quantifying the binding affinity and other interaction parameters between sfGFP and the GFP-enhancer nanobody, we will enhance our understanding of their interaction and potential in protein research.

The biophysical methods used to measure the interaction between the nanobody and sfGFP are appropriate for solution-phase conditions that mimic physiological environments. They avoid linking one of the binding partners to a solid support, as would be required, for example, when using surface plasmon resonance methods, which also investigate the thermodynamics of interactions. Environmental conditions can be readily adjusted to monitor the effect of ionic strength, pH, analyte concentration, and temperature, and additives like small molecules and reductants can be used to further modulate binding behavior. For fluorescence methods, it is necessary to have a fluorophore. If intrinsic fluorescence is not available as in the case of sfGFP, one of the molecules must be fluorescently labeled, which could change its behavior and influence its molecular parameters. In such a case it is advantageous to label the smaller molecule, because bigger hydrodynamic shifts are observed when the smaller molecule forms a complex with an invisible larger molecule. Combining the results from all techniques will provide a comprehensive profile of the composition, thermodynamic and hydrodynamic properties of the free and complexed molecules.

General Considerations

When studying molecular interactions, the affinity and stoichiometry of the interaction need to be determined. Additional questions may include the kinetics of the reaction, which is beyond the scope of this study. In order to provide accurate quantitative information about affinity and stoichiometry, it is essential to first characterize the molecules by themselves. Monomeric molar mass, the potential for self-association and oligomerization, as well as aggregation propensity, need to be determined, and accurate molar concentrations must be measured. Furthermore, a buffer system that does not interfere with the detection in any of these methods and is conducive to the ideal behavior of all involved molecules must be chosen. In order to eliminate the potential for undesirable off-target reactions and interference from contaminants it is important to verify the purity of the reaction partners before attempting to interpret the biophysical measurements. Experimental designs must be developed that maximize the signal and observe the dynamic range of each instrument. As a consequence of this requirement selected methods may be inappropriate for a particular system. The investigator must be aware of the limitations and applicable operational ranges of each technique before attempting to interpret the resulting data. In our research we distinguish qualitative methods relying on standards or reference materials (e.g., gel electrophoresis, size-exclusion chromatography), and first-principles methods which rely on fundamental physical laws that can be mathematically modeled (typically by differential equations). First-principles methods do not require reference materials in order to permit interpretation of the experimental data, and allow derivation of molecular parameters from the fitted equations.

The primary object of investigation of an interaction is the dissociation equilibrium constant k_D and the stoichiometry of an interaction between two molecules *A* and *B*. The equilibrium constant describes the affinity of the interaction, and *m* and *n* describe the molecule's stoichiometries. The k_D is expressed in molar concentration and is described by Eq. 1:

$$k_D = \frac{[A]^m[B]^n}{[A_mB_n]} \quad Eq.\ 1$$

The measurement of the k_D requires the determination of the concentrations [*A*], [*B*], and [A_mB_n]. The equilibrium described by Eq. 1 is subject to mass action. Because k_D is a constant, any change in the concentration of *A* or *B* also induces a change in the concentration of A_mB_n. This means that multiple observations with different concentrations of *A* and *B* can be used to predict the same k_D value. While a single ratio of [*A*] and [*B*] is sufficient for the determination of the k_D, a titration of *A* and *B* is frequently employed to generate multiple distinct observations for the same property, enhancing the confidence in the result. This is especially important when the tested ratio is far from the k_D concentration. The most reliable results are obtained when the measurements include multiple concentrations in the vicinity of the k_D concentration and both below and above the k_D concentration. It is worth noting that more complex, and often intractable, situations can be encountered when multiple competing reactions, or multiple reaction partners, or molecules with different oligomerization states and stoichiometries exist simultaneously. Then it is often difficult or impossible to separate the contribution of each component to the overall observed signal. Another consideration should be the dynamic range of the technique. For determination of thermodynamic constants a method with a large dynamic range is more likely able to cover the entire isotherm of the reaction.

Concentration Determination: In order to determine k_D concentrations, an accurate molar concentration must be available for each reactant. For protein or nucleic acid solutions, the concentration of each biopolymer is readily determined by ultraviolet-visible (UV-vis) spectroscopy. Non-absorbing molecules can often be quantified using refractive index methods. To obtain molar extinction coefficients for proteins, the absorbance at 280 nm can be measured and converted to molar concentration by the method of Gill and von Hippel [10], which estimates the molar extinction coefficient at 280 nm from the sequence of the protein and the number of tryptophan, tyrosine, phenylalanine, and disulfide bonds in cysteine residues contained in the sequence. These values can be predicted by programs like UltraScan [11] or Sednterp [12]. Additional information can be obtained by refractive index methods. A comprehensive review of methods to determine accurate molar extinction coefficients for proteins, including glycosylated proteins, can be found in [13]. Once a molar extinction coefficient is available, absorbance scans from a protein dilution series can be fitted globally to an intrinsic extinction curve with UltraScan. This curve is then normalized with the known molar extinction coefficient at 280 nm, providing a molar extinction coefficient profile for all wavelengths included in the absorbance scans. When measuring the absorbance of macromolecular solutions, it is imperative to only trust values that are in the linear range of the instrument. This range depends on the detector and light intensity at each wavelength. Typically, measurements between 0.1-1.0 OD can be trusted to be linear for most instruments with xenon light sources, and wavelengths between 210-650 nm. We also recommend using 10 mm pathlength quartz cuvettes. Another consideration is the absorbance contribution of the buffer components. Each buffer should be measured by itself in a spectrophotometer that has been blanked with ddH_2O. The sample should be measured after blanking the instrument with the buffer. The combined OD from both the buffer and the sample should be within the dynamic range of the detector, and typically not exceed 1.0 OD at the selected wavelength. Buffer components such as nucleotides, reductants, EDTA, or HEPES can add considerable absorbance at some wavelengths, and should be avoided for most spectroscopic observations. One potential challenge is that carbohydrates and lipids typically do not absorb in the accessible wavelength range. If they are large enough, they will scatter light, producing a pseudo-absorbance signal that does not scale with concentration, but with the 6^{th} power of the particle radius. Here, refractive methods should be chosen instead for a more accurate concentration determination. Additional details can be found in [31, 14].

Temperature and Buffer: Equilibria of interactions are affected by temperature and buffer conditions.

Therefore, the observed k_D values may be different if multiple experiments are performed under non-identical conditions. In this study all experiments were performed in the same buffer and near the same temperature (20 ºC) to avoid variations in the observed k_D values. It is important to note that thermodynamic parameters as well as partial specific volume can be quite sensitive to ionic strength, pH, and the presence of reductants or detergents. Variation of these parameter can offer insights into the chemistry and types of forces involved in the interactions.

Materials and Methods

FCS measurements were performed at the Biospectroscopy Core Research Facility at the Center for Biomolecular Structure and Dynamics at the University of Montana. Proteins sfGFP and the nanobody were expressed and purified at the Integrated Structural Biology Core at the University of Montana (Missoula, Montana). All other biophysical characterization was performed at the Canadian Center for Hydrodynamics at the University of Lethbridge (Lethbridge, Alberta).

Ultraviolet-Visible Spectroscopy (UV-vis): Prior to conducting MW-AUC experiments, a spectral analysis of each protein and the complex mixtures was performed to create an intrinsic extinction coefficient spectrum. These spectra were used to determine the optimal sample concentration required for the MW-AUC experiment, assuring that the absorbances of the mixed samples were within the dynamic range of the detector (0.1-1.0 OD). They were also used for the spectral deconvolution of the MW-AUC data. First, the UV-visible absorbance of each protein was measured across the range of 220-550 nm at room temperature (22 °C) with a ThermoFisher Genesys 50S bench-top spectrophotometer in a 1 cm pathlength quartz cuvette. To obtain the intrinsic extinction coefficient spectrum, a serial dilution was scanned for each protein. Data points within the dynamic range of the spectrophotometer (0.1-1.0 OD) were globally fitted with the "Spectrum Fitter" module in UltraScan and scaled to the extinction coefficients of the proteins (SI 1, SI 2) [15]. An extinction coefficient of 83,300 OD/mol was used for sfGFP at 488 nm which was experimentally determined by Pédelacq et al. [5], and 28,545 OD/mol was taken for the nanobody at 280 nm based on the method by Gill and von Hippel using the Expasy ProtPram tool [10, 16]. The intrinsic extinction coefficient spectrum of the proteins had random residuals (SI 1, SI 2), ensuring that they can be used as basis spectra for the spectral decomposition of the complex. An overlay of the molar extinction coefficient profiles for all samples is shown in Figure 1. Prior to AUC analysis, UV-visible spectra of the mixtures were collected and fitted to a sum of Gaussians [15]. The fit of the mixtures also showed random residuals (SI 4, SI 3). Measurements of the mixtures were performed after approximately 30 minutes of incubation for the mixtures. To verify the composition of the mixtures, their fits were loaded into the "Spectrum Decomposition" module in UltraScan, and decomposed into the basis spectra for nanobody and sfGFP (see Figures 2 and 6).

Microscale Thermophoresis (MST): Taking advantage of the intrinsic fluorescence of sfGFP, the molecular motion of both free and complexed sfGFP can be monitored to measure diffusion in a temperature gradient. An infrared (IR) laser is used to induce a precise spatial temperature distribution in the sample, which facilitates thermophoretic movement observed via fluorescence excitation and emission. The IR laser allows for high-precision heating of the solution in a capillary, which requires only 2 µL of sample for each titration point. The thermophoretic properties of the molecule changes in the temperature gradient, causing a concentration gradient of the molecule to be established. When the laser is turned off, the temperature rapidly equilibrates, and the molecules diffuse back to their equilibrium state. Because diffusion is inversely proportional to size, the speed of the back diffusion is a sensitive indicator of the weight average size of the complexed and free analytes. A titration series of the nanobody is performed, while maintaining a constant concentration of sfGFP, allowing MST to accurately determine binding affinities between sfGFP and nanobody in their unbound and bound states. The methodology of MST is further discussed in [17]. Measurements of the titration points were

performed after approximately 15 minutes of incubation. *MST measurements were conducted using a NanoTemper Monolith NT.115 instrument to track the binding of sfGFP to nanobody by measuring the molecular diffusion in a temperature gradient. Initially, the stock solution of sfGFP was diluted to a final concentration of 75 nM in phosphate-buffered saline and the nanobody was prepared at an initial concentration of 10 µM in phosphate-buffered saline. A two-fold serial dilution of the nanobody was performed across 16 samples, with the concentration of nanobody ranging from 10 µM to 152 pM. Each of these dilutions was then mixed in a 1:1 ratio with the 75 nM sfGFP solution, resulting in a final sfGFP concentration of 37.5 nM in each mixture and nanobody ranging from 5 µM to 76 pM. 2 µL of each titration point were loaded into separate NanoTemper Monolith NT.115 Series capillaries. The MST measurements were executed at a constant temperature of 22°C, with the MST power set to medium. The excitation power was adjusted to 5% using the Nano – BLUE setting. The experiments were performed in triplicate. Data analysis was conducted with the MO. Affinity Analysis software.*

Isothermal Titration Calorimetry (ITC): ITC is a label-free, first principal technique used to directly measure the heat absorbed or released when an interaction occurs. The heat is equal to the enthalpy (ΔH) of that reaction, which provides information about other thermodynamic parameters of biomolecular interactions, including the dissociation constant (k_D), association constant (k_a), entropy (ΔS), and stoichiometry (n). It is important to note that n can only be accurately determined when accurate sample concentrations are available, and all molecules are fully active. During the ITC experiment, a microcalorimeter detects heat changes associated with the binding events between macromolecules. This is achieved by titrating the nanobody from an injection syringe into a sample cell containing sfGFP, alongside a reference cell filled with water. The calorimeter monitors temperature differences between these cells upon binding and uses feedback-controlled heaters to maintain a constant temperature. ITC requires extensive preparation time, and sensitivity to buffer conditions and is not ideal for interactions with no or very low enthalpy changes because they cannot be effectivelymeasured using ITC. Another consideration that must be made when applying ITC is material consumption. A volume of up to 430 µL is required for the binding partner and 150 µL for the ligand, with concentrations as high as 500 µM are required, depending on the interaction. Further information can be found in [18]. ITC measurements were performed using an Affinity ITC instrument (TA Instruments). The nanobody was concentrated to 96 µM and sfGFP was diluted to 15 µM in phosphate-buffered saline. Both samples were degassed and equilibrated to a temperature of 25°C prior to loading. The ITC cell was filled with 300 µL of sfGFP, meeting the minimum volume requirement, and 80 µL of nanobody was loaded into the injection syringe. An initial injection of 0.4 µL of nanobody into the cell was used to stabilize the system. Subsequently, 1.5 µL injections of nanobody were administered into the cell across 32 total injections, spaced by 120-second intervals, with stirring maintained at 125 rpm. The resulting data were analyzed with the NanoAnalyze Software (TA Instruments).

Multi-Wavelength Analytical Ultracentrifugation (MW-AUC): Multi-wavelength AUC adds a second dimension to standard single-wavelength detection, where any molecules with distinct absorbance spectra can be resolved by spectral separation in addition to the traditional hydrodynamic separation [14, 19]. For the sfGFP-nanobody interaction, the unique spectral profile of sfGFP with a peak absorbance at 488 nm clearly distinguishes it from the nanobody, which lacks the 488 nm excitation peak. The spectral properties of each molecule are first determined by using ultraviolet-visible spectroscopy (UV-Vis). When mixtures are measured in a MW-AUC experiment, a hydrodynamic characterization of all components by sedimentation velocity analysis is complemented by the spectral separation of the sedimentation signal, which produces separate molar concentration signals for each analyte in the mixture. Based on the molar composition of both sfGFP and nanobody, complexes and their molar ratios can be identified, and the molar masses of each species can be calculated based on hydrodynamic characterization, which measures the sedimentation (s) and diffusion (D) coefficients. Molar mass (M) conversion requires knowledge of the partial specific volume,$\bar{v}$(Eq. 2).

$M = \frac{sRT}{D(1-\bar{v}\rho)}$ *Eq. 2*

The partial specific volume was estimated by UltraScan based on the protein sequence for individual molecules, and weight-averaged values are used for complexes, consistent with their stoichiometry as described in [20, 21]. When the sfGFP and nanobody complex is formed, the resulting composite spectra reflect proportional contributions from each involved solute, providing direct access to stoichiometries of binding as long as molar extinction coefficients are known accurately. Additional information about MW-AUC can be found in [14, 22, 23]. Using the UV-vis spectral analysis as a guide, the proteins were diluted with phosphate-buffered saline to achieve an absorbance within the dynamic range of the detector at their maximum absorbance peaks (280 nm and 488 nm). Measurements of all samples were performed after one hour of rotor temperature equilibration. Each of the proteins was measured individually as a control along with two mixtures of sfGFP and nanobody, a 1:1 and 1:2 molar ratio of sfGFP:nanobody in a Beckman-Coulter Optima AUC at the Canadian Center for Hydrodynamics at the University of Lethbridge, which was calibrated for chromatic aberration [24]. The molar concentrations derived are based on the assumed extinction coefficients. Therefore, the accuracy of k_D concentrations and stoichiometries is dependent on the accuracy of the molar extinction coefficients used. 460 µL of each sample were loaded into 2-channel epon centerpieces and fitted with quartz windows. Samples were measured in an An60Ti rotor at 47 krpm for 12.5 hours at 20 °C in intensity mode. The mixtures were measured in multi-wavelength mode, measuring between 260-290 nm and 475-499 nm at every second wavelength. According to UV spectroscopy, these wavelength ranges appeared to be minimally affected by hypo-/hyper-chromic shifts upon complexation. Nanobody and sfGFP controls were measured at 280 nm and 488 nm, respectively. To optimize data collection, only a single cell was scanned when collecting data in multi-wavelength mode. Individual wavelength datasets were analyzed according to methods described earlier Nanobody and sfGFP mixtures were analyzed by the two-dimensional spectrum analysis (2DSA) [***25***] to the iterative step, followed by a Monte Carlo refinement [***26***].

Data acquisition and analysis were performed with Ultrascan-III v. 7285 according to methods described in [14, 15]. For MW-AUC data, only the 280 nm dataset was used to estimate the meniscus position; this position was then applied to the datasets from all other wavelengths belonging to the same channel. Due to the sequential acquisition of multi-wavelength scans obtained from Beckman optics, a time synchronization is required, and performed with the UltraScan "Optima MWL Fit Simulation" module, followed by the spectral decomposition with the UltraScan "MWL Species Fit" module as described in [14]. A van Holde-Weischet analysis was used to plot diffusion-corrected integral sedimentation coefficient distributions from the deconvoluted datasets [27].

Fluorescence AUC: ***Fluorescence detection in an AUC is made possible by the FDS detector from Aviv Biomedical, installed in a Beckman Proteomelab XLA at the University of Lethbridge. Excitation is achieved with a 488 nm laser and a confocal radially scanning microscope is used to observe the fluorescence signal as a function of radius [28]. Fluorophores that can be excited at 488 nm include the GFP variants, making this interaction study suitable for fluorescence AUC. Because the entire signal reflects only the fluorescent molecule, this technique offers exquisite selectivity, even in an impure solution where the presence of other protein molecules would obscure the signal of interest. To measure interactions with fluorescence AUC, a titration series with a constant amount of fluorophore is measured, and the amount of complex formed is measured as a function of concentration. Because complexed molecules are larger in molar mass, a positive shift in sedimentation coefficient is indicative of complex formation. Hydrodynamic analysis can be used to derive molar masses, further supporting the formation of a complex. Fluorescence data were analyzed with UltraScan according to methods described in [15], using the 2DSA [25], followed by Monte Carlo analysis [26]. A weight-average sedimentation coefficient from the Monte Carlo analysis was determined for each titration point from 100 Monte Carlo iterations. The weight-average***

sedimentation coefficients were subsequently globally fitted to a sigmoidal function. Using the MST and ITC results as a guide, mixtures of 100 nM sfGFP and nanobody concentrations of 0.25 nM, 0.43 nM, 1 nM, 2.3 nM, 3 nM, 4 nM, 9 nM, 19 nM, 48 nM, 100 nM, 102 nM, 105 nM, 115 nM, 120 nM nM were prepared and measured at 50 krpm for 9 hours at 20 ºC. Measurements of all samples were performed after one hour of rotor temperature equilibration. The fluorescence detection gains were adjusted to produce a response below 4000 counts to stay within the dynamic range of the detector.

Fluorescence correlation spectroscopy (FCS): FCS complements MW-AUC by providing orthogonal measurements of the diffusion coefficients of free and complexed sfGFP by a first principle method. In FCS, fluorescent molecules are excited and observed in a tiny focal volume, where the dynamics and interactions of biomolecular processes can be observed at the single-molecule level. The fluctuations in fluorescence intensity are measured, providing information about the diffusion coefficient, hydrodynamic radius, and local concentration. By employing FCS, we can gain a deeper understanding of the dynamic properties of these protein interactions, further validating the data obtained from other biophysical techniques used in this research. For more information refer to [29]. Fluorescence correlation spectroscopy measurements were performed in a similar manner to Steele et al. [30]. After sample preparation, m***easurements of the mixture was performed after 30 minutes of incubation.*** Data were acquired over three or four replicates by time-correlated-single-photon counting (TCSPC) on a PicoQuant MicroTime 200 microscope with a 40X water immersion objective. All samples were excited with a vertically polarized 485nm pulsed diode (LDH-D-C-485) operating at a 40hz repetition rate and an optical power of 2 µW at the objective. The spectral width of this laser is between 2 and 8 nm. Emissions were filtered through a 30 µm pinhole and a 488nm long-pass filter (AHF/Semrock BLP488-R) and collected by a PicoQuant Hybrid PMT. The confocal volume was calculated by measuring Alexa488 (XFD488 acid, AAT Bioquest), a sample with a known diffusion coefficient of 435 $\mu m^2/s$ [31]. All experiments were performed in triplicate. Eq. 3 details the model used to calculate the effective volume. In this equation κ represents the length-to-diameter ratio of the focal volume, *D* represents diffusion coefficient, and τ_{Diff} represents the diffusion time of the species.

$$V_{EffD} = \kappa[D4\tau_{Diff}\pi]^{\frac{3}{2}} \quad Eq.\ 3$$

sfGFP was measured at a concentration of 10 nM in PBS for two minutes to minimize photobleaching. A count-rate of 5,000 cps was maintained for the duration of the acquisition. In the presence of nanobody, the molar ratio was 2:1 nanobody:sfGFP. FCS data were fitted with PicoQuant SymphoTime 64 version 2.3. A one component pure diffusion model displayed in Eq. 4 was used to fit and calculate the translational diffusion coefficients. In Eq. 4 n_{Diff} is the number of independently diffusing species, ρ is the contribution of the i^{th} diffusing species, *t* represents time, τ_{Diff} represents the diffusion time of the i^{th} species, and κ represents the length to diameter ratio of the focal volume.

$$G(t) = \sum_{i=0}^{n_{Diff}-1}\left(\frac{\rho[i]}{[1+\frac{t}{\tau_{Diff}[i]}][1+\frac{t}{\tau_{Diff}[i]\kappa^2}]^{0.5}}\right) \quad Eq.\ 4$$

The translational diffusion coefficient, *D*, is then calculated from Eq. 5, where w_0 is the effective lateral focal radius at $(1/e)^2$ intensity and τ_{Diff} is the diffusion time of the i^{th} species.

$$D = \frac{w_0^2}{4\tau_{Diff}} \quad Eq.\ 5$$

Room temperatures during data collection varied between 20-23 ˚C. Therefore, all diffusion are coefficients corrected to a $D_{20,W}$ value by estimating the approximate viscosity of the solution at 20 ˚C. This is shown in Eq. 6.

$$D_{20^\circ C} = D_{T,B}\left(\frac{\eta_{T,B}}{\eta_{20^\circ C}}\right) Eq.\ 6$$

Eq. 6 is used to correct any measured translational diffusion coefficient D determined at any temperature T and in buffer B to standard conditions at 20 ˚C and water. The diffusion coefficient at a given temperature is described by D and the viscosity of the solvent at a given temperature is described by η..

SEC-MALS: Size exclusion chromatography is a preparative separation technique, fractionating mixtures of molecules based on their size. In-line detectors for UV absorptivity, refractive index, multi-angle static light scattering (MALS), and dynamic light scattering (DLS) together provide information on the concentration and molar mass, as well as the diffusion coefficients of the separated molecules. While chromatographic separation by itself requires a set of appropriate reference standards to aid in the interpretation of the results, the combination of the in-line detectors provide a first-principle characterization, largely eliminating the need for reference materials. For this study, an KW402.5-4F Shodex HPLC column was used. The MALS analysis was performed using a Dawn® (Wyatt Technology Corporation, Santa Barbara, CA, USA) equipped with 18 detector angles and a 658 nm laser. Refractive index was measured with an Optilab® refractometer (Wyatt Technology Corporation, Santa Barbara, CA, USA). Samples were prepared at concentrations of 72.5 µM (sfGFP), 149.2 µM (nanobody), and 69.9 µM (complex) and centrifuged at 10 krpm for 3 minutes to remove any aggregates. 100 µL of each sample was injected into the column. The molecular weight was determined as described by the manufacturer using the Astra v8.0.0.25 software using Eq. 7.

$$M = \frac{R_0}{K^* c}$$
$$where: K^* = \frac{4\pi^2 n_0^2 (dn/dc)^2}{\lambda_0^4 N_A} Eq.\ 7$$

R_0 is the Rayleigh ratio at angle $\theta=0$, c is the concentration in mg/mL, n is the refractive index of the solvent, λ_0 is the wavelength of the laser in vacuum, dn/dc is the differential refractive index of the solution in mL/g, and N_A is Avogrado's number. A dn/dc value of 0.16 mL/g was used for the molecular weight determination. The diffusion coefficient D is derived from the scattering autocorrelation function g of time increment τ (Eq. 8).

$$g(\tau) = B + \beta e^{(-2\Gamma\tau)} Eq.\ 8$$

where B is the baseline of the correlation function at infinite delay, β is the correlation function amplitude at $\tau=0$, and Γ is the decay time. Γ is directly proportional to D (Eq. 9).

$$D = \frac{\Gamma}{\left(\frac{4\pi n}{\lambda_0}\sin(\theta/2)\right)^2} Eq.\ 9$$

The Stokes Einstein equation (Eq. 10) can be used to interpret the diffusion coefficient D as a diffusing sphere with the hydrodynamic radius r_h. Where k_B is the Boltzmann constant, T is temperature, and η is the solvent viscosity.

$$D = \frac{k_B T}{6\pi\eta r_h} Eq.\ 10$$

Temperature and buffer correction of measured diffusion coefficients to standard conditions for water at 20 ºC can be performed with Eq. 6. Additional information can be found in [32, 33].

Purification of the anti-GFP nanobody (GFP-enhancer): Anti-GFP nanobody was a gift from Martin Spiess ("pET24a-VHH-TEV-mCherry "Addgene plasmid #117752) and protein was purified following

a modified protocol published in [34] with an additional TEV cleavage step to remove the mCherry tag. AntiGFP nanobody-TEV-mCherry-6xHis nanobody was expressed in SHuffle T7 Express cells (NEB C3029) in Terrific Broth media supplemented with 0.4% w/v glucose and 50 ug/mL Kanamycin. After growing shaking 1L cultures to an OD_{600} = 0.8 at 37 degrees C, the temperature was dropped to 18 degrees C and cultures were induced with 150 μM IPTG for 16 hours. 4 L of cultures were harvested by centrifugation at 4000xg and lysed in 300 mL lysis buffer (50mM Tris pH 7.5, 300mM NaCl, and 10mM imidazole) with 1mM PMSF, 10mg lysozyme, and 1mg DNase in an Avestin Emulsiflex c5 cell disruptor (Avestin, Quebec, Canada). Lysate was clarified at 19,000 x g for 1hr and flowed over two 5ml Histrap FF nickel columns (GE Cytiva 17-5255-01) and washed thoroughly with 300-800 mL of lysis buffer. Protein was eluted with a gradient up to 500mM imidazole in lysis buffer and eluted at 250mM imidazole. Eluted protein was buffer exchanged using a 10 kDa MWCO centrifugal filter into PBS buffer and treated with TEV protease at a ratio of 6 mg TEV to 90 mg of AntiGFP nanobody-TEV-mCherry-6xHis overnight at 4 degrees C. Proteolytically cleaved protein was passed over loose nickel-NTA beads equilibrated in PBS, and the antiGFP nanobody flow through was concentrated to 7mg/ml in a 10kDa MWCO centrifugal filter prior to size exclusion in PBS buffer.

Purification of Super-Folder GFP: 6xHis-sfGFP was purified following a modified protocol published in [35] with an additional TEV cleavage step to remove the 6xHistidine tag. sfGFP was expressed in BL21 DE3 *E. coli* (New England Biolabs) in LB media supplemented with 100 ug/mL Carbenicillin. After growing/shaking 1L cultures to an OD_{600} = 0.8 at 37 degrees C, the temperature was dropped to 18C and cultures were induced with 150 μM IPTG for 16 hours. 2 L of culture was harvested by centrifugation at 4000xg and lysed in 300 mL lysis buffer (50mM Tris pH 7.5, 300mM NaCl, and 10mM imidazole) with 1mM PMSF, 10mg lysozyme, and 1mg DNase in an Avestin Emulsiflex c5 cell disruptor (Avestin, Quebec, Canada). Lysate was clarified at 19,000 x g for 1hr and flowed over two 5ml Histrap FF nickel columns (GE Cytiva 17-5255-01) and washed thoroughly with 1L of lysis buffer. Protein was eluted with a gradient up to 500mM imidazole in lysis buffer and eluted at 250mM imidazole. Eluted protein was buffer exchanged using a 10 kDa MWCO centrifugal filter into PBS buffer and treated with TEV protease at a ratio of 6 mg TEV to 100 mg sfGFP at 4C. Proteolytically cleaved protein was passed over loose nickel-NTA beads equilibrated in PBS, and the sfGFP flow through was concentrated to 7mg/ml in a 10kDa MWCO centrifugal filter prior to size exclusion in PBS buffer.

Results

UV-Vis: **Decomposition of the 1:1 mixture** shows a composition of 55.73% nanobody and 44.27% sfGFP (Figure 2A). The decomposition of the 2:1 mixture shows a composition of 67.52% nanobody and 32.48% sfGFP (Figure 2B). Both mixtures were confirmed to be close to the intended ratios. Previously, the effect of the nanobody binding on the sfGFP UV-vis spectrum has not been studied in detail. We do see minor hyper- and hypochromic shifts in the UV-Vis absorption spectrum as a result of the association with the nanobody (see Figures 2A and B), suggesting that in our experimental conditions sfGFP chromophore is deprotonated without nanobody association.

MST: The MST experiment resulted in a k_D of 1.53 nM with a standard error of 3.98 nM. The signal-to-noise ratio was 14.1 with no detected aggregates or ligand-induced photobleaching rate changes. The results are shown in Figure 3.

ITC: The raw heat release data per injection and the integrated binding isotherm are shown in Figure 4. The integration points were fit using the NanoAnalyze independent model, which was combined with a blank constant model for baseline correction. The independent binding model assumes that each binding site on the macromolecule binds the ligand independently, without influencing the binding affinity of other sites. The enthalpy of the reaction was -46.48 kJ/mol. From the measured result of the enthalpy, the k_D, n, and entropy were able to be calculated. A k_D of 1.000 ± 0.633 nM, an n of 0.917, and an entropy

of 13.76 J/mol·K with a 95% confidence level was obtained. The signal-to-noise ratio for the fit of the resulting data was 117, with a standard deviation of 0.4.

MW-AUC: The multi-wavelength AUC results are shown in Figure 5 (integral distributions) and Figure 6 (differential distributions). Both controls of sfGFP and nanobody show vertical integral sedimentation profiles, indicating that the reactants are mostly homogeneous and of high purity. Fits of these data resulted in signal-to-noise ratios between 128 to 300, depending on wavelength. The analysis reveals three distinct species: free sfGFP, sedimenting at 2.84 *s*, free nanobody, sedimenting at 1.72 *s*, and their 1:1 complex, sedimenting at 3.35 *s*. Molar masses measured by AUC for these species are in excellent agreement with the predicted molar masses from sequence, with 26.7 kDa for sfGFP (26.8 kDa from sequence), 15.1 kDa for the nanobody (15.2 kDa from sequence), and 41.6 kDa (42.1 kDa from sequence) for the complex (see Table 1). The decomposition achieves a precise determination of each species' partial concentrations, which are highly consistent with the prediction obtained from the UV-vis analysis. The sedimentation profiles of deconvoluted sfGFP in the mixture exhibit a shift in the sedimentation coefficient distribution to 3.35 *s*, demonstrating that the total amount of sfGFP is bound to the nanobody in both 1:1 and 1:2 mixtures. In the 1:1 mixture, sfGFP has a concentration of 9.35 µM, constituting 42.5% of the total mixture concentration while in the 1:2 mixture, the sfGFP concentration decreases to 7.02 µM, representing 32.0% of the total concentration. Similarly, the nanobody in the 1:1 mixture shifts from free to bound sedimentation (1.72 s to 3.31 *s*), with a small portion of the boundary showing an excess of free nanobody in the sedimentation profile, as expected. The nanobody concentration in the 1:1 mixture is 12.66 µM, accounting for 57.5% of the total concentration and explaining the observed slight excess of free nanobody. In the 1:2 mixture, the nanobody remains in excess with a concentration of 14.93 µM corresponding to 68.0% of the total concentration. This shift between free and complexed nanobody is distinctly observed in Figure 5. The frictional ratios derived from the analysis provide additional insights into the shape of sfGFP and its interactions with the nanobody, with sfGFP showing the most globular species with f/f_0 1.28, and nanobdy and complex both slightly more extended with an f/f_0 of 1.31. Free sfGFP and nanobody exhibit larger diffusion coefficients than the 1:1 complex, with the nanobody recording the largest diffusion coefficient, consistent with their molar masses (Table 1). All fits produced random residuals.

Fluorescence AUC: The weight averaged sedimentation coefficients from the 2DSA-Monte Carlo analysis for each sfGFP-nanobody mixture were determined with UltraScan and plotted against the predictions of molar fractions of nanobody mixed with sfGFP (Figure 7A). The k_D was measured using a sigmoidal function fit of the plot and reported a value of 1.72 nM, in good agreement with the other reported K_d values (Figure 7B, Table 1). At 100 nM sfGFP concentration, the instrument recorded signal-to-noise ratios ranging between 70-100, with ratios generally increasing when the sfGFP was fully complexed with nanobody enhancer, consistent with the higher fluorescent yield expected for a fully formed complex. All fits produced rand om residuals.

FCS: For the purpose of measuring the translational diffusion coefficients of sfGFP with and without nanobody bound, we performed fluorescence correlation spectroscopy. The diffusion coefficients measured by FCS change with particle size, so it was expected that complexed sfGFP would have a larger hydrodynamic radius with a lower diffusion coefficient. In these experiments the nanobody was in excess of sfGFP at a 1:2 ratio of sfGFP to nanobody. Because of the nanomolar K_d it is assumed that approximately all sfGFP is complexed in the presence of nanobody. These data are shown in Figure 8. Graph A depicts the autocorrelation curve of sfGFP in the absence of nanobody, which when fit to a single diffusion coefficient model produced a diffusion coefficient of 105.9 +/- 2.96 $\mu m^2/s$. With sfGFP saturated by nanobody, graph B shows a similar autocorrelation curve that produces a diffusion coefficient of 89.6 +/- 3.91 $\mu m^2/s$ due to the change in MW upon nanobody binding. Both autocorrelation curves, with and without nanobody, were normalized with the highest data point in each set represented as unity. This is displayed in graph C with the red curve (nanobody bound) being slightly right-shifted

due to slower diffusion.

SEC-MALS and DLS: Analytical SEC-MALS was employed as a complementary biophysical technique to measure molecular weight and diffusion coefficients of the samples. The refractive index of the phosphate-buffered saline was measured to be 1.331 mL/g and was used to determine the absolute solute concentrations for the molecular weight calculations. The molecular weights determined by SEC-MALS were 16.90 ± 1.04 kDa for the nanobody, 27.90 ± 0.71 kDa for sfGFP, and 34.26 ± 1.67 kDa for the complex in a 1:1 molar ratio mixture. Diffusion coefficients were measured as 103.1 ± 4.4 $\mu m^2/s$ for the nanobody, 84.1 ± 2.3 $\mu m^2/s$ for sfGFP, and 78.6 ± 2.5 $\mu m^2/s$ for the complex. The results are summarized in Figure 9.

Discussion

UV-Vis: ***When bound to sfGFP, the nanobody enhances the fluorescence of sfGFP and contributes to hyper- and hypochromic shifts of the absorbance spectrum of sfGFP when in complex (see Figures 1 and 2). This effect must be considered when calculating molar ratios. As a consequence, minor deviations in the molar extinction coefficient in the complexed state should be expected. Accordingly, our results show a small excess of nanobody in both mixtures, which could be both explained through pipetting errors and by minor deviations in the actual extinction coefficients for the complexed state (Figures 2A and B).***

MST: The reported k_D of 1.53 nM lies in a low nanomolar range, showing that the binding between sfGFP and GFP-enhancer is very strong and specific to a stable complex. This is corroborated by Figure 3, which exhibits a steep increasing sigmoidal jump followed by a sharp plateau, typical of strong binding events, with few data points in between the bound and unbound species. Because we approach the range of sensitivity limits of the Monolith NT.115 (1 nM-500 mM), the potential for increased measurement error increases, supported by the relatively large error margin of 3.98 nM. This could indicate the possibility of a picomolar k_D. For future MST studies, a Monolith NT.115 Pico would be more appropriate. Despite the large error, we can confirm that the k_D would not exceed a low nanomolar range as the results are corroborated with ITC. MST excels by requiring minimal sample amounts, and a short time for the experiment and analysis, but users need to be aware of capillary fouling and sample aggregation, which may demand additional optimization.

ITC: Similarly to the MST data, the sigmoidal fit in the ITC results exhibits a steep transition, suggesting a very strong and specific interaction between sfGFP and nanobody. The ITC data, as shown in Figure 4, presents a k_D of 1.000 ± 0.633 nM, which aligns closely with the MST results. This consistency between two different techniques supports the reliability of the low nanomolar k_D. However, it is important to consider the inherent limitations of ITC when measuring extremely tight binding interactions. The sensitivity of the instrument typically prevents accurate determination of k_D values below 1 nM. Therefore, the actual k_D for this interaction might be in the picomolar range, which the ITC could not resolve due to its detection limits. While ITC could theoretically measure picomolar k_D values using specialized methods, doing so would require extremely low concentrations that could exceed the dynamic range of the instrument, making it a challenging to recover the exact k_D of the interaction. While the k_D of the sfGFP and nanobody cannot be accurately reported by ITC due to its tight (<1nM) affinity, the enthalpy of complex formation is in good agreement with that reported for eGFP and GFP-enhancer binding also determined by ITC. These values differ only by 3% at -44.98 kJ/mol (-10.75 kcal/mol) at 25C with eGFP [36] and -46.48kJ/mol (-11.11 kcal/mol) at 25 degrees C with sfGFP. This small difference may be due to the several folding-enhancing mutations in sfGFP [5] that are close to the interface with GFP-enhancer nanobody, including A206V affecting a direct side-chain contact of the nanobody [36, 37]. Since A206 is part of the hydrophobic patch involved in the interaction, and valine substitution does not alter its hydrophobic nature, the minimal effect on the association enthalpy is not

surprising. Limiting factors of ITC include the high sample requirements, and the challenge of keeping molecules soluble in high concentration measurements, while maintaining the exact same buffer for both components.

MW-AUC: **By combining a traditional hydrodynamic AUC characterization with a multi-wavelength analysis, it is possible to determine the molar stoichiometry of any complex formed. Using the basis spectra obtained from the UV-Vis analysis, the AUC signal belonging to each hydrodynamic species was deconvoluted, providing precise molar concentrations for each component in the mixture. Hydrodynamic separation additionally aids in the identification and quantification of each species, whether contributing to a complex, or left unbound in solution. Furthermore, an orthogonal validation of any free or complexed species is possible from the calculation of the molar mass derived from the sedimentation and diffusion coefficients, combined with the sequence-derived partial specific volume (weight averaged for complex species). It needs to be stressed that any molar concentration is only as accurate as the available molar extinction coefficient, and accuracy of the molar mass is dependent on the accuracy of the partial specific volume of each species, which is typically only estimated from sequence, but subject to variations caused by the buffer. For the case of nanobody and sfGFP we were able to conclusively verify a 1:1 stoichiometry of the complex, supportive of the ITC results (Figures 5 and 6, and Table 1). Because of dynamic range limitations in the detector, sample concentrations were too high to accurately measure the k_D concentrations. Nevertheless, the high signal-to-noise level obtained at these higher concentrations afforded very high precision for hydrodynamic parameters and partial concentrations. Diffusion coefficients available from MW-AUC methods are complementary to FCS and DLS measurements, but some values differed. When the identity of the hydrodynamic species can be assigned, for example from the molar mass or the spectral profile, Eq. 2 (the Svedberg relationship) is an excellent validation tool for the reliability of the measurement. Using the sedimentation coefficients, which can be assigned with very high confidence, the diffusion coefficients measured with a different technique also must reproduce the expected molar mass. This is discussed further in the FCS and SEC-MALS/DLS sections. The relatively low dynamic range of the UV/visible absorbance detector constrains the accessible concentration range, and limits the k_D range that can be observed. Furthermore, complex forming molecules will need to contribute to the overall absorbance within the dynamic range, and provide approximately equal signal in order to be accurately measured. Unlike any other method, sedimentation velocity experiments excel in distinguising the presence of contaminants and additional oligomerization reactions, while other techniques may only detect weight-averages of all species present.**

Fluorescence AUC: **Under favorable conditions and with sufficiently high fluorescence yield, fluorescence technology can extend the dynamic concentration range of AUC to at least 1 order of magnitude lower concentrations than can be achieved with UV-visible detection, facilitating measurements of tight binding interactions. While the concentration of 100 nM sfGFP concentration in our instrument was barely low enough to estimate a k_D in the low nanomolar range, these concentrations provide sufficient data quality and the results are still in good agreement with both ITC and MST, which both also were at the limit of their dynamic range (Figure 7). Because non-fluorescent nanobodies are not visible in the fluorescence AUC measurement, it is not possible to report on the hydrodynamic parameters of unlabeled nanobody with this technique. As in MST and ITC, a steep jump in the signal is observed in the vicinity of the k_D, but this measurement still relies on knowing the concentration of nanobody accurately from the titration. Clearly, because the nanobody is invisible in the fluorescence experiment, it cannot be measured in this experiment, and the results are only as reliable as the concentration measurements of the unlabeled molecule in the titration. The same consideration applies to the MST and ITC experiments. Compared to MW-AUC, F-AUC suffers from lower signal-to-noise**

ratios, although the dynamic range for concentration for F-AUC is significantly larger, and the exquisite selectivity of fluorescence detection provides clear advantages when working with complex or impure solutions.

FCS: We used FCS to measure the translational diffusion for orthogonal verification of the diffusion coefficient obtained from AUC and DLS. Our diffusion coefficients for free sfGFP were 10% higher for sfGFP and 25% for the complex compared to AUC, and 26% higher for sfGFP and about 14% higher for the complex when compared to DLS (Table 1). Notably, the values produced by FCS were from a different preparation of enhancer nanobody than was used in AUC and DLS (Table 1). However, previous comparisons between our FCS and AUC instruments produced agreement within 2% when the same protein preparation was used (data not shown). Although our FCS values were corrected for the average temperature and buffer conditions during measurement, small fluctuations in stage temperature could have increased this error. Because the diffusion measurements for FCS are consistently higher than for both AUC and DLS, a systematic error in the experimental setup is possible. Moreover, unlike SEC-MALS or AUC, individual molecules are not separated in FCS, and weight-average diffusion coefficients are observed when multiple components are present in a mixture. If there is any unbound sfGFP in the complexed sample, the observed diffusion coefficient would be elevated, which could partially explain the discrepancy for the complex. A good sanity check of the observed values is the calculation of molar mass and frictional ratios, f/f_0, by combining the FCS-measured diffusion coefficients using Eq. 2 with the sedimentation coefficient from the AUC experiments, which are measured with high confidence, and the partial specific volume derived from sequence. The values we recorded systematically produce lower molar masses and f/f_0 values than both DLS and AUC, also suggesting a systematic error in the FCS measurements.

Other fluorescent proteins and eGFP have been used as viscometers for various cellular compartments, and values for *D* of eGFP in water are reported in [38, 39]. These values range from 87-130 $\mu m^2/s$ and were measured at different temperatures with various methods [31, 38, 40, 41, 42]. Typically these data are not reported as $D_{20,W}$ values. Thus, these values are hard to compare with the present work unless corrected. The approach taken within the current work provides a standardization of diffusion values produced by multiple techniques. It is also important to consider that these literature values were obtained with different implementations of FCS (scanning vs fixed point) along with adjacent measures of diffusion such as fluorescence recovery after photobleaching. Subtle differences in experimental setup as well as data acquisition, sample purity, and analysis could account for the range of reported diffusion coefficients. For example, Petrasek and Schwille utilized two-photon excitation along with scanning FCS to minimize photobleaching of the GFP [31]. While care was taken to minimize photobleaching of sfGFP in the current work, we did not use scanning FCS or have a two-photon excitation source available to us. Additionally, the small alterations to the sequence and structure of sfGFP as compared to eGFP could explain some of the differences in diffusion between sfGFP and eGFP.

Additional considerations can be made about the induction of the triplet state during FCS measurements. As stated, care was taken to keep the laser power relatively low and minimize photobleaching. In doing this, we do not perceive there to be significant triplet state within the autocorrelation functions for sfGFP. When fitting our data to a triplet state model, fits are not adequate, and some parameters are undeterminable (data not shown). Based on this we determined the pure diffusion model to be most representative of the sfGFP hydrodynamics. There has been a report that GFP mutants can enter a dark state similar to the triplet state, which coul Monolith NT.115 Pico d account for diffusion numbers that skew higher [43].

SEC-MALS/DLS: The data obtained from SEC-MALS provides valuable information on the molecular weight and diffusion properties of biomolecules, but accuracy is limited by the resolution of size-based separation. Unlike MW-AUC, where superb 3-dimensional separation can be achieved (sedimentation,

diffusion, and spectral properties), resolution in SEC-MALS is challenging when mixtures of molecules of similar size need to be measured. High purity is essential to ensure molecular weight determinations are not influenced by oligomers, aggregates or contaminants. As can be seen in Figure 9D, separation between sfGFP and the complex in SEC-MALS is very minor, despite a 56% difference in molar mass. In this study, the molecular weights determined from MALS for pure nanobody and pure sfGFP were in excellent agreement with the mass determined from their sequences (sfGFP: 4%, nanobody: 11%, complex: 18%) and by AUC (sfGFP: 4%, nanobody: 12%, complex: 17%). The MALS-determined molecular weight of the complex was underestimated by approximately 7 kDa, closely matching the error trends seen in the FCS results for the elevated diffusion coefficients. While the solutions with a 1:1 molar ratio of sfGFP and nanobody were prepared using the same methods as in the UV-Vis and MW-AUC experiments, the superior separability by MW-AUC provides the most reliable result when characterizing composition. Both analyses indicated an excess of a smaller molecule in the mixture, suggesting that the SEC-MALS measurement may have included free nanobody or sfGFP in addition to the complex, lowering the apparent mass. Similarly, the DLS measurement produced a diffusion coefficient slightly larger than the one observed by AUC. It is expected that poor resolution in the SEC column could provide a weighted average *D* value for a mixture of free nanobody or free sfGFP and the 1:1 complex. Despite this limitation, SEC-MALS can effectively distinguish the nanobody, sfGFP, and the complex, as demonstrated in Figure 9. However, because this technique alone cannot fully separate complex mixtures, additional size exclusion chromatography over a larger column volume prior to analyses could yield more accurate results by ensuring complete separation of free nanobody from the complex. For sfGFP alone, DLS reported a lower *D* value than AUC, while FCS reported a larger *D* value than AUC.

Summary

Protein-protein interactions are best studied using solution-based biophysical methods, where molecules can interact dynamically, and without physical constraint. The performance of multiple methods was examined for a tight binding interaction (k_D ~ 1 nM). As we have demonstrated, a high degree of confidence can be obtained about the stoichiometry, molar mass, k_D, and composition of an interacting system. We found that MST, fluorescence AUC and ITC agreed very well on the k_D of the interaction, although this k_D concentration is close to the limit of their dynamic range. In those cases, instrumentation that would extend the dynamic range to lower concentrations (Monolith NT.115 Pico for MST experiments), or surface plasmon resonance, as was applied in a related study [44], would be recommended. Unfortunately, this equipment was not available to us. While all of our methods are measuring interactions free in solution, techniques such as surface plasmon resonance rely on fixing the substrate to a solid support, which could impact the measurements when compared to free solution methods. All other methods could not be used for measuring the k_D, however, ITC and MW-AUC both agreed on a 1:1 stoichiometry. MALS detection of molar mass was in excellent agreement with molar masses derived from sequence, but only if the sample was already highly purified. For the complex, the presence of additional unbound molecules could only be resolved by MW-AUC, which also provided the most reliable composition analysis. AUC and column chromatography approaches utilize UV/visible and/or interference optics for detection, which provide a direct metric for the concentration of the sample, either by optical density or refractive index. This is a strong advantage for measuring composition or k_D, compared to methods that rely on the user to provide the concentration. MW-AUC was also the most consistent when providing diffusion coefficients and molar masses. In this instance, FCS produced larger diffusion coefficients when compared with DLS and MW-AUC. However, the FCS data was not from the same preparation of protein that was used in DLS and MW-AUC making it difficult to tease out if the error was systematic with regard to the instrumental setup for FCS, or could be attributed to differences in heterogeneity of the proteins. UV-visible spectroscopy provided very accurate composition information for mixtures when spectral decomposition was employed, and clearly indicated chromatic

shifts in the spectrum when complexes were examined. Standard deviations for MW-AUC and fluorescence AUC were overall the smallest, due to the large number of data points collected. While some methods provide information for more than one parameter, the confidence limits for such parameters vary greatly based on experimental conditions and sample properties, which is true for all techniques. Table 2 provides an overview of the molecular parameters available from the techniques applied here.

Acknowledgments

This research was supported by the Canada Research Chairs program C150-2017-00015 (to B.D.) and CRC-2021-00420 (to T.R.P), the National Institutes of Health grants 1R01GM120600 (to B.D.) and R01GM109053 (to E.V), and the Canadian Natural Science and Engineering Research Council Discovery Grant DG-RGPIN-2019-05637 (to B.D) and DG-RGPIN-2022-03391 (to T.R.P), and RTI-2023-00004 and RTI-2020-00090 (to T.R.P. and B.D.). The Canadian Center for Hydrodynamics is funded by the Canada Foundation for Innovation grant CFI-37589 (to B.D.), CFI-41008 (to B.D. and T.R.P) and CFI-37155 (to T.R.P). UltraScan supercomputer calculations were supported through NSF/XSEDE grant TG-MCB070039N (to B.D.). The sfGFP and nanobody enhancer protein were expressed and purified by the Integrated Structural Biology Core, while fluorescence correlation spectroscopy was performed by the BioSpectroscopy Core at the University of Montana. Both cores are funded by NIGMS grant P30GM140963 to the Center for Biomolecular Structure and Dynamics at the University of Montana.

List of Abbreviations:

PPI:	Protein-Protein Interactions
GFP:	Green Fluorescent Protein
sfGFP:	Superfolder Green Fluorescent Protein
DNA:	DeoxyriboNucleic Acid
RNA:	Ribonucleic Acid
MST:	Micro-Scale Thermophoresis
ITC:	Isothermal Titration Calorimetry
AUC:	Analytical Ultracentrifugation
MW-AUC:	Multi-wavelength Analytical Ultracentrifugation
F-AUC:	Fluorescence Analytical Ultracentrifugation
SEC-MALS:	Size Exclusion Chromatography – Multi-Angle Light Scattering
DLS:	Dynamic Light Scattering
FCS:	Fluorescence Correlation Spectroscopy
k_D:	Dissociation Constant
k_A:	Association Constant
ddH_2O:	double-distilled water
EDTA:	EthyleneDiamineTetraAcetic acid
HEPES:	4-(2-HydroxyEthyl)-1-PiperazineEthaneSulfonic acid
UV-vis:	*Ultraviolet-Visible Spectroscopy*
OD:	Optical Density
IR:	Infrared
ΔH:	*Enthalpy of the reaction*
ΔS:	*Entropy of the reaction*
n:	*Stoichiometry*
D:	*Diffusion Coefficient*
s:	*Sedimentation Coefficient*

M:	*Molar Mass*
:	*Partial Specific Volume*
r_h*:*	*Hydrodynamic Radius*
k_B*:*	*Boltzmann constant*
Γ:	Decay Time
T:	Temperature
η:	Solvent Viscosity
dn/dc:	*Differential Refractive Index*
2DSA:	*Two-dimensional Spectrum Analysis*
TCSPC:	*Time Correlated Single Photon Counting*
MWCO:	*Molecular Weight Cut Off*
PMSF:	*PhenylMethylSulfonyl fluoride (Protease Inhibitor)*
PBS:	*Phosphate Buffered Saline*
kDa:	*kilo Dalton*

CRediT author statement

Aysha K. Demeler: conceptualization, data curation, formal analysis, investigation, methodology, writing – original draft, visualization
James Bosco: Data curation, conceptualization, methodology, formal analysis, investigation, writing – original draft
Matthew J. Sydor: Data curation, formal analysis
Michelle Nemetchek: Data curation, review and editing, writing – original draft
Saeed Mortezazadeh: Software
Liam Kerr: Data curation, formal analysis
Sophia Bird: Data curation, formal analysis
Roza Gabdullina: Data curation
Cindee Yates-Hansen: Data curation, review and editing
Levi McClelland: Data curation, resources, supervision
Ekaterina Voronina: Funding, resources, supervision, review and editing
Trushar R. Patel: Funding, resources, supervision, review and editing
Borries Demeler: Project administration, funding, conceptualization, resources, supervision, formal analysis, investigation, methodology, writing – original draft, review and editing.

ORCID

0009-0006-7170-6045 – Aysha K. Demeler
0009-0006-7141-8705 – James Bosco
0000-0002-8738-4451 – Matthew J. Sydor
0000-0003-3524-952X – Michelle Nemetchek
0000-0001-6437-6953 – Saeed Mortezazadeh
0000-0002-5459-4639 – Liam Kerr
0009-0007-1629-5762 – Sophia Bird
0009-0006-4910-5219 – Roza Gabdullina
0000-0001-8116-2586 – Cindee Yates-Hansen
0000-0002-0868-8925 – Levi McClelland
0000-0002-0194-4260 – Ekaterina Voronina
0000-0003-0627-2923 – Trushar R. Patel
0000-0002-2414-9518 – Borries Demeler

Table 1: Summary of experimental results for all techniques, values in parentheses indicate the standard error.

Technique	sfGFP	Nanobody	1:1 Complex
Partial Specific Volume			
Sequence (ml/g)	0.7311	0.7108	0.7238
Molecular Weight			
Sequence (kDa)	26.9	15.2	42.1
MW-AUC (kDa)	26.7 (± 1.75)	15.1 (± 0.74)	41.6 (± 1.1)
SEC-MALS (kDa)	27.9 (± 0.71)	16.9 (± 1.0)	34.3 (± 1.7)
Diffusion Coefficient			
MW-AUC ($\mu m^2/s$)	96.2 (± 4.2)	104 (± 3.6)	71.8 (± 1.9)
SEC-DLS ($\mu m^2/s$)	84.1 (± 2.3)	103.1 (± 4.4)	78.5 (± 2.5)
FCS ($\mu m^2/s$)	105.9 (± 3.0)	-	89.6 (± 3.9)
Sedimentation Coefficient			
MW-AUC (x 10^{13} s)	2.84 (0.044)	1.72 (± 0.042)	3.35 (± 0.026)
Frictional Ratio, f/f_0			
MW-AUC (x 10^{13} s)	1.28	1.31	1.31
k_D			
MST (nM)	1.52 (± 3.98)		
ITC (nM)	1.00 (± 0.633)		
F-AUC (nM)	1.72 (± 0.028)		

Table 2: Overview of molecular parameters available from techniques discussed in this manuscript:

	k_D	Concentration	Molar Mass	Stoichiometry	Diffusion	Composition
UV/Visible		X				
MST	X					
ITC	X			X		
MW-AUC	X	X	X	X	X	X
F-AUC	X		X	X	X	X
FCS		X			X	
MALS		X	X	X		
DLS		X			X	

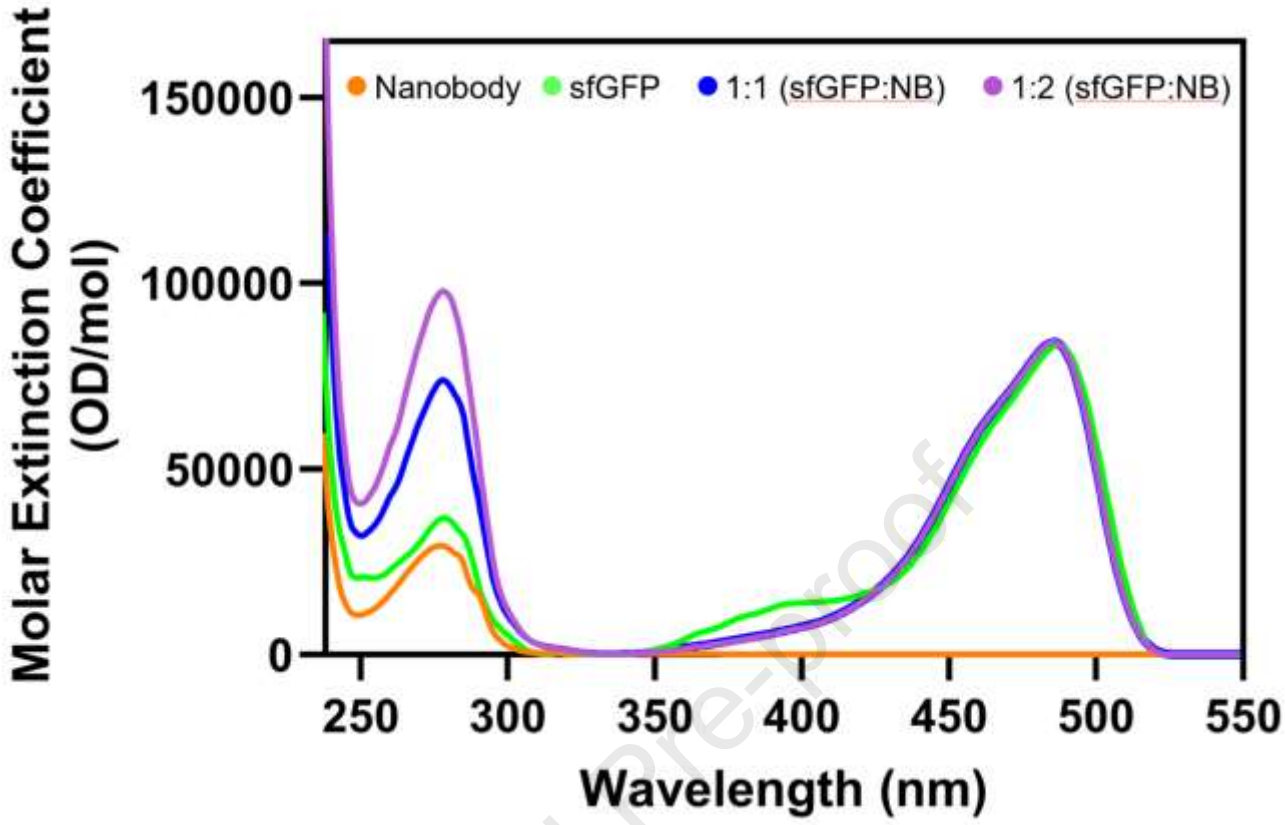

Figure 1: Molar extinction coefficient spectral profiles for sfGFP (green), nanobody (orange), combined 1:1 molar ratio mixture (blue), and 1:2 molar ratio mixture (sfGFP:nanobody, purple).

Figures

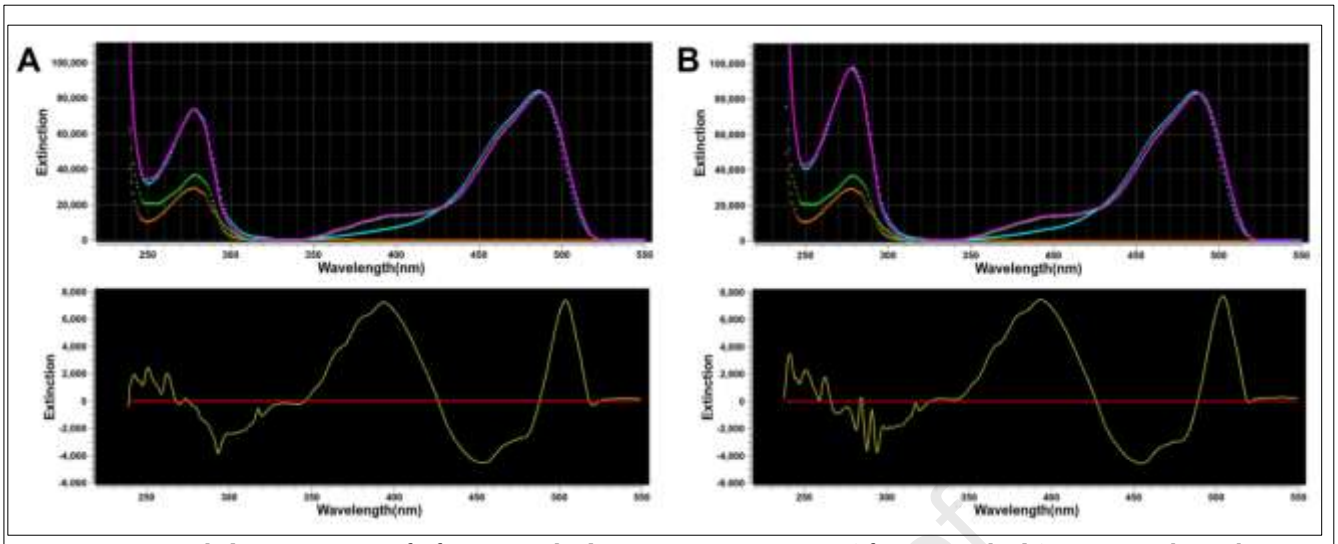

Figure 2: Spectral decomposition of sfGFP:nanobody mixtures. ***A:*** *1:1 M (sfGFP:nanobody) mixture where the target spectrum (blue) is the intrinsic extinction coefficient spectrum of the mixture, the basis spectra are the intrinsic extinction coefficient spectra of sfGFP (green) and nanobody (orange) and the fit of the target spectrum (magenta) provides the solution of the decomposition (top). The decomposition indicates a composition of 44.27 ± 0.99% of sfGFP and 55.73 ± 1.26% of nanobody. The residuals are shown in yellow (bottom). The relatively large deviations are an indication of hyper- and hypo-chromic shifts in the absorbance spectrum upon complex formation.* ***B:*** *1:2 M (sfGFP:nanobody) mixture where the target spectrum (blue) is the intrinsic extinction coefficient spectrum of the mixture, the basis spectra are the intrinsic extinction coefficient spectra of sfGFP (green) and nanobody (orange) and the fit of the target spectrum (magenta) provides the solution of the decomposition (top). The decomposition indicates a composition of 32.48 ± 0.99% of sfGFP and 67.52 ± 2.06% of nanobody. The residuals are shown in yellow (bottom). The relatively large deviations are an indication of hyper- and hypo-chromic shifts in the absorbance spectrum upon complex formation, which show a nearly identical pattern as the 1:1 molar ratio fit shown in* ***A****.*

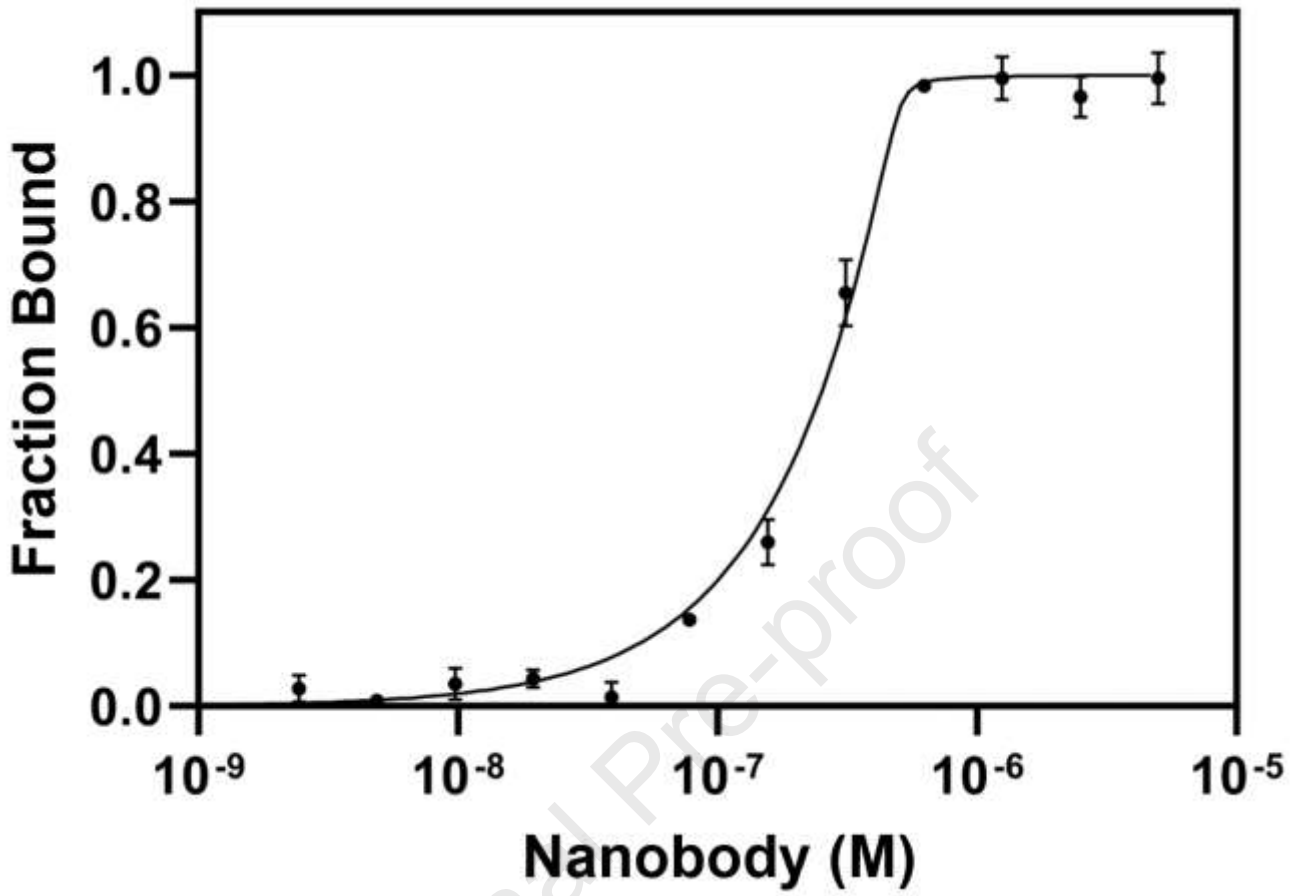

Figure 3: Microscale thermophoresis measurement for the interaction between sfGFP and nanobody. The nanobody was titrated up to a maximum concentration of 10 µM into a constant amount of sfGFP at a concentration of 37.7 nM and was measured after a minimum of a 20 minute incubation time at room temperature (22 °C). The dissociation constant was determined to be 1.53 ± 3.98 nM (reduced X^2 = 1.548, Std. error of regression = 0.459). The error bars are based on triplicate measurements.

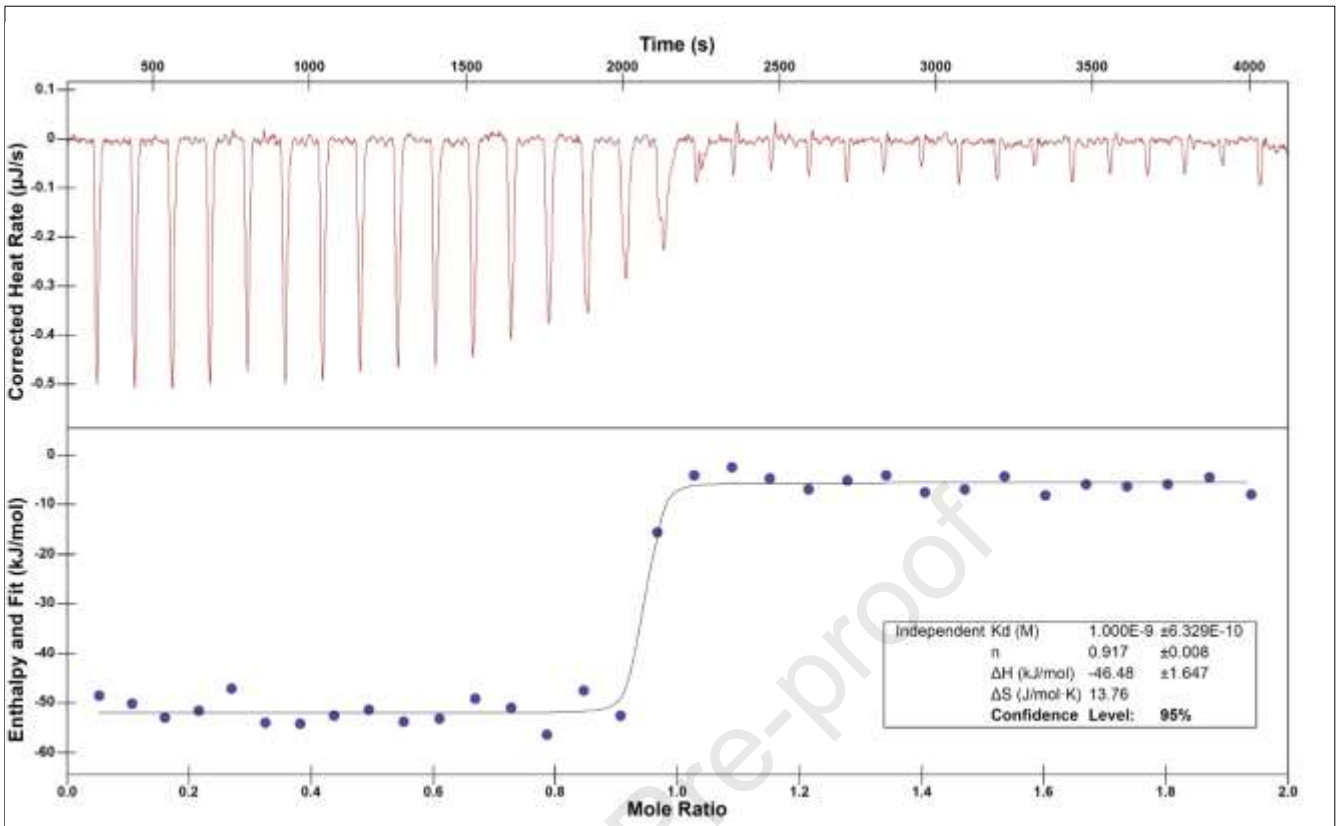

Figure 4: Isothermal titration calorimetry measurement for the interaction between sfGFP and nanobody. Exothermic enthalpy plots showing (top) the raw data of 32 titrations with a 120 second interval of 96 µM nanobody to 15 µM sfGFP and (bottom) the integrated enthalpy using an independent model as a function of the molar ratio of the nanobody with the derived thermodynamic parameters including dissociation constant (k_D), stoichiometry (n), enthalpy (ΔH), and entropy (ΔS).

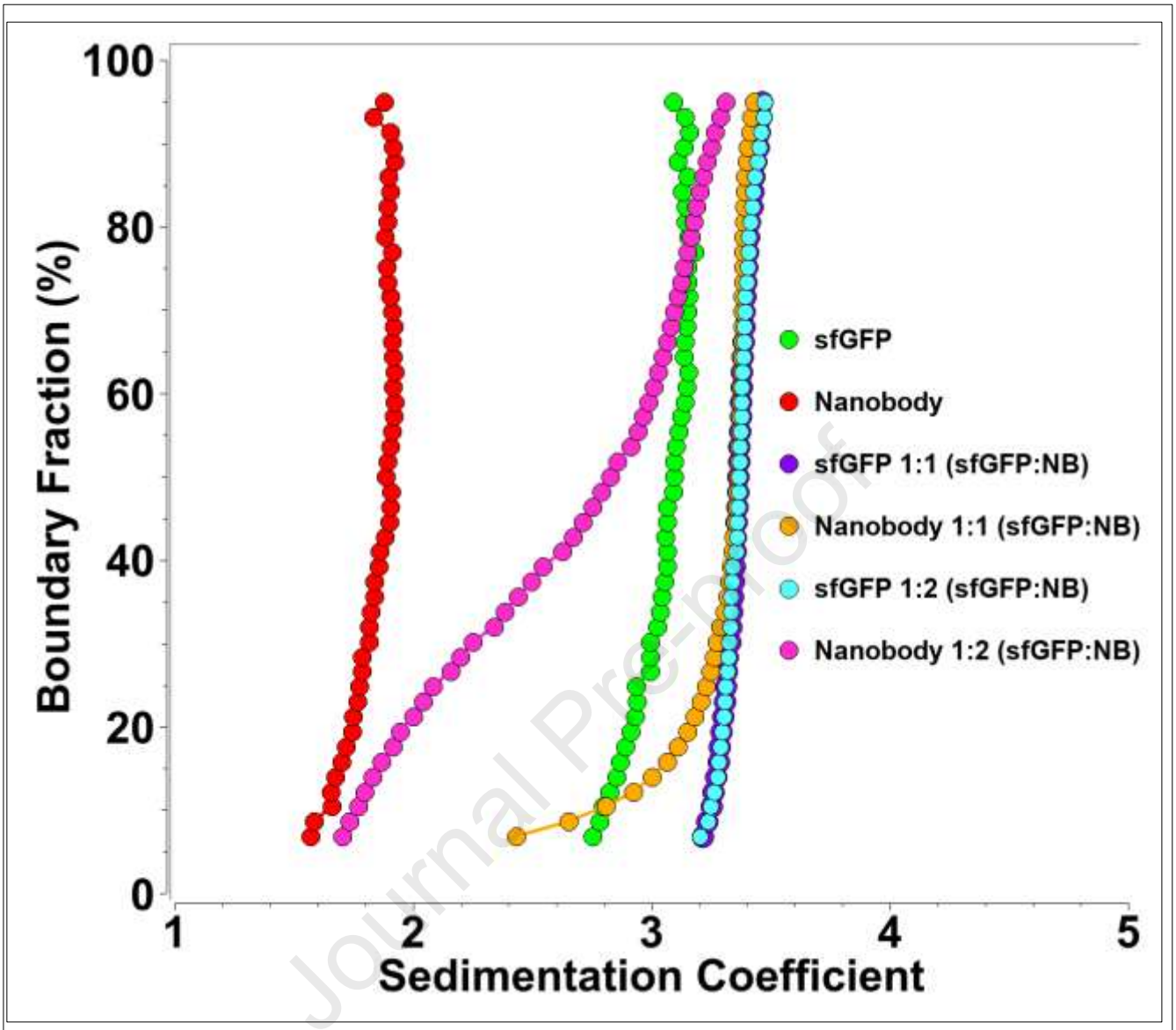

Figure 5: Multi-wavelength AUC results, integral representation: Van Holde Weischet distributions of sedimentation velocity 2DSA-IT of the nanobody control in red (RMSD = 2.11e-3), and sfGFP in green (RMSD = 2.53e-3), and the multi-wavelength deconvolution signals of sfGFP in the 1:1 M mixture (purple), sfGFP in the 1:2 mixture (cyan), nanobody in the 1:1 M mixture (orange), and nanobody in the 1:2 M mixture (pink). The lines in this figure are for visualization purposes while the dots are representative of the measured sedimentation coefficients for each part of the boundary fraction.

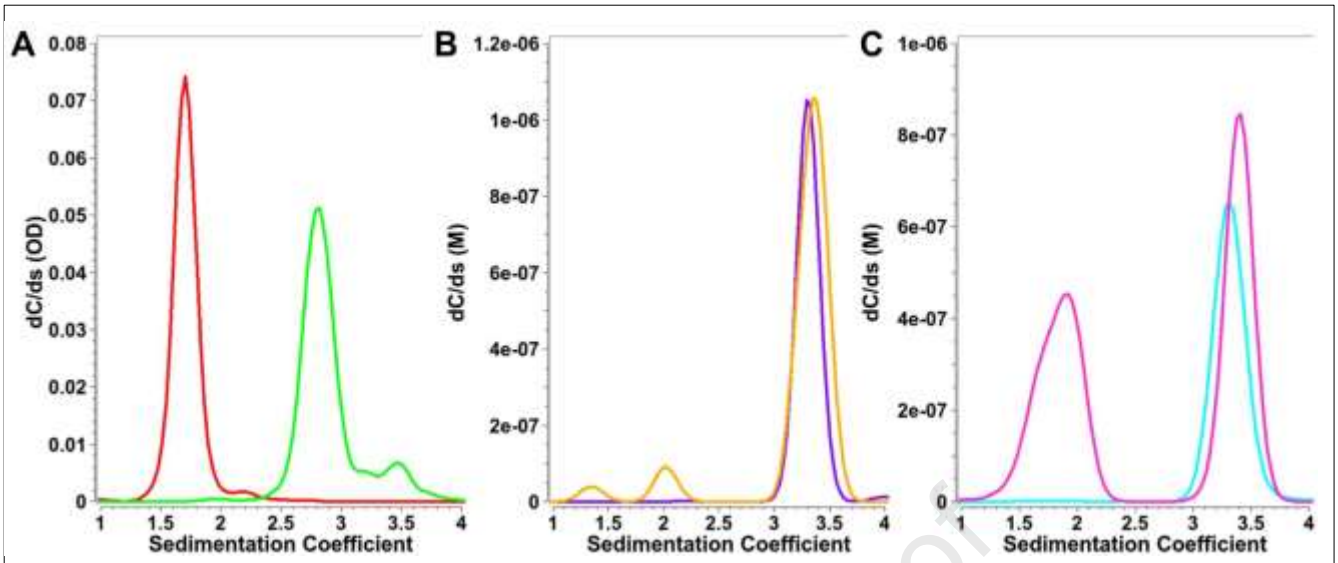

Figure 6: Multi-wavelength AUC results, differential representation: ***A:*** *Sedimentation velocity 2DSA-Monte Carlo controls of nanobody in red and sfGFP in green with RMSDs of 2.03e-3 and 2.47e-3 respectively.* ***B:*** *Deconvolution of the 1:1 M mixture of nanobody (orange) and sfGFP (purple).* ***C:*** *Deconvolution of the 1:2 M mixture of nanobody (pink) and sfGFP (cyan).*

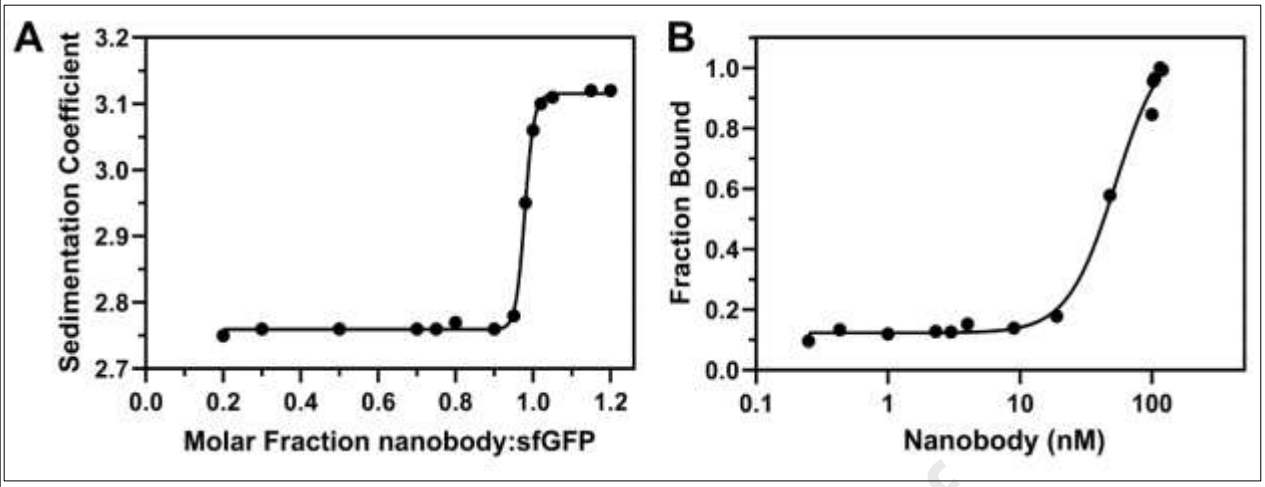

Figure 7: Fluorescence AUC analysis: ***A:*** *Sigmoidal fit to weight-averaged sedimentation coefficients from 100 iterations of the 2DSA-Monte Carlo analysis for individual titration points plotted against the molar fraction of nanobody to sfGFP.* ***B:*** *Sigmoidal fit of fraction bound nanobody to sfGFP plotted against the concentration of titrated nanobody in nM.*

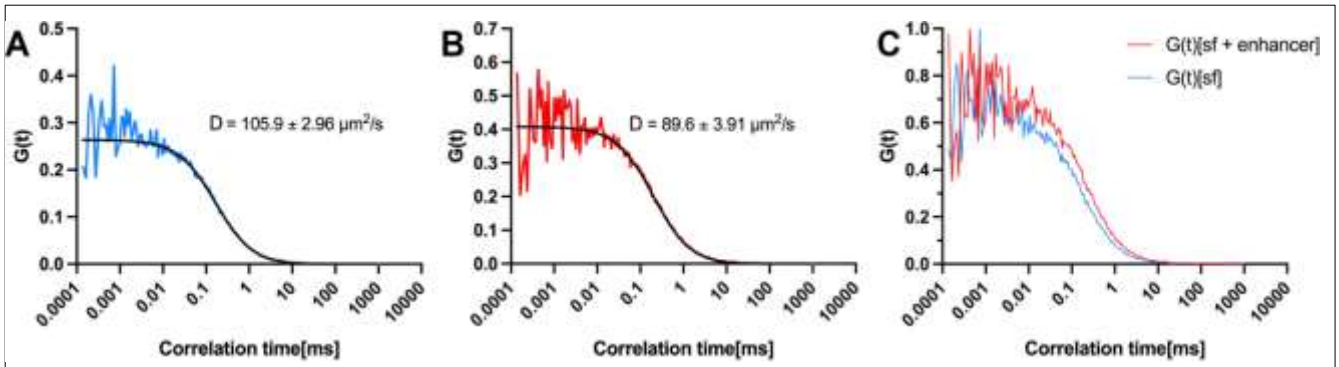

Figure 8: Autocorrelation Curves Acquired by Fluorescence Correlation Spectroscopy. ***A:*** *sfGFP without enhancer nanobody.* ***B:*** *sfGFP with enhancer nanobody.* ***C:*** *sfGFP with and without nanobody, normalized and plotted on the same graph. All curves and fits are from one representative measurement. The black lines are a one-component pure diffusion model.*

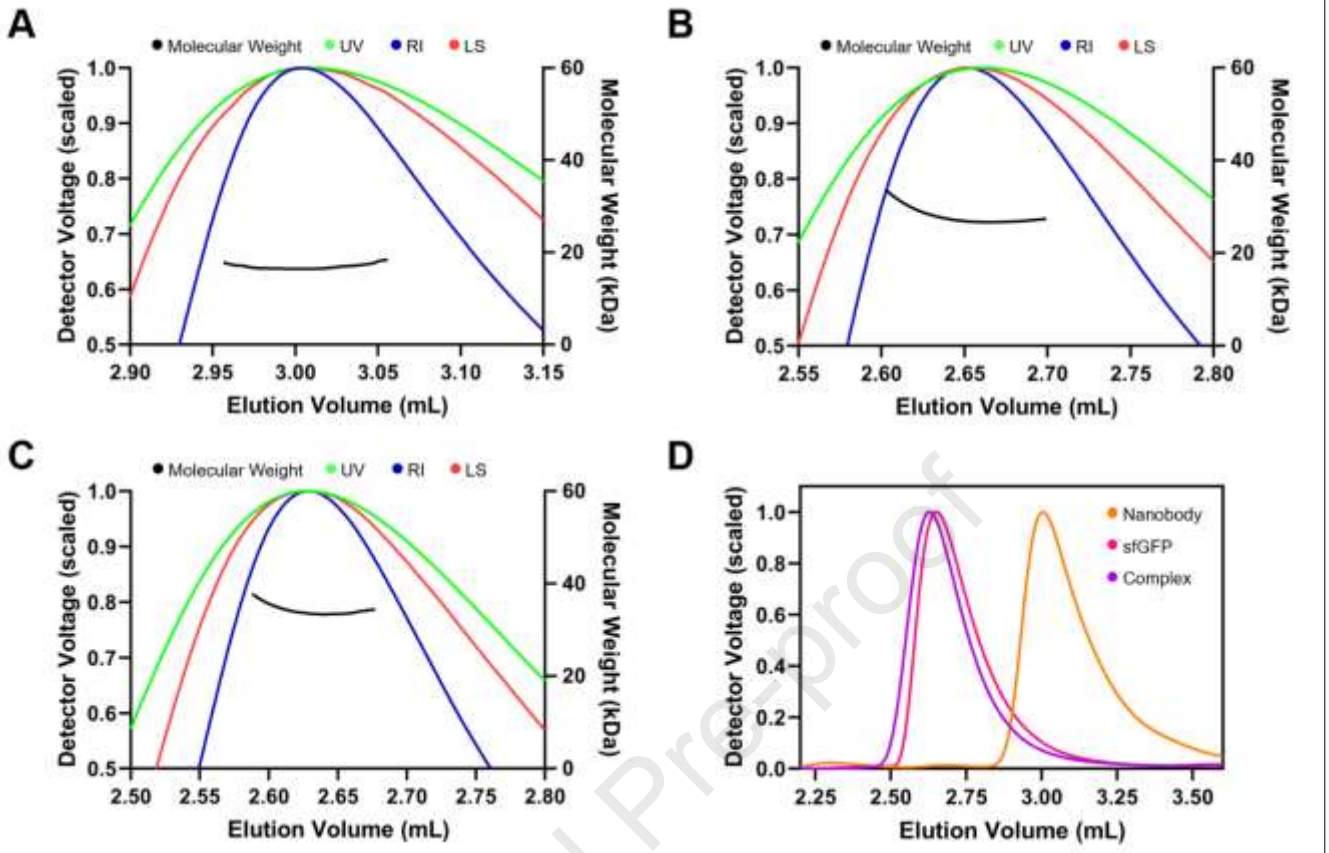

Figure 9: SEC-MALS data showing UV in green, refractive index (RI) in blue, and light scattering (LS) in red, with the calculated molecular weight in black for A nanobody, B sfGFP, and C 1:1 molar ratio for the complex. D shows the refractive index traces for the complex (purple), sfGFP (pink), and nanobody (orange), depicting the shifts in elution volume for each species.

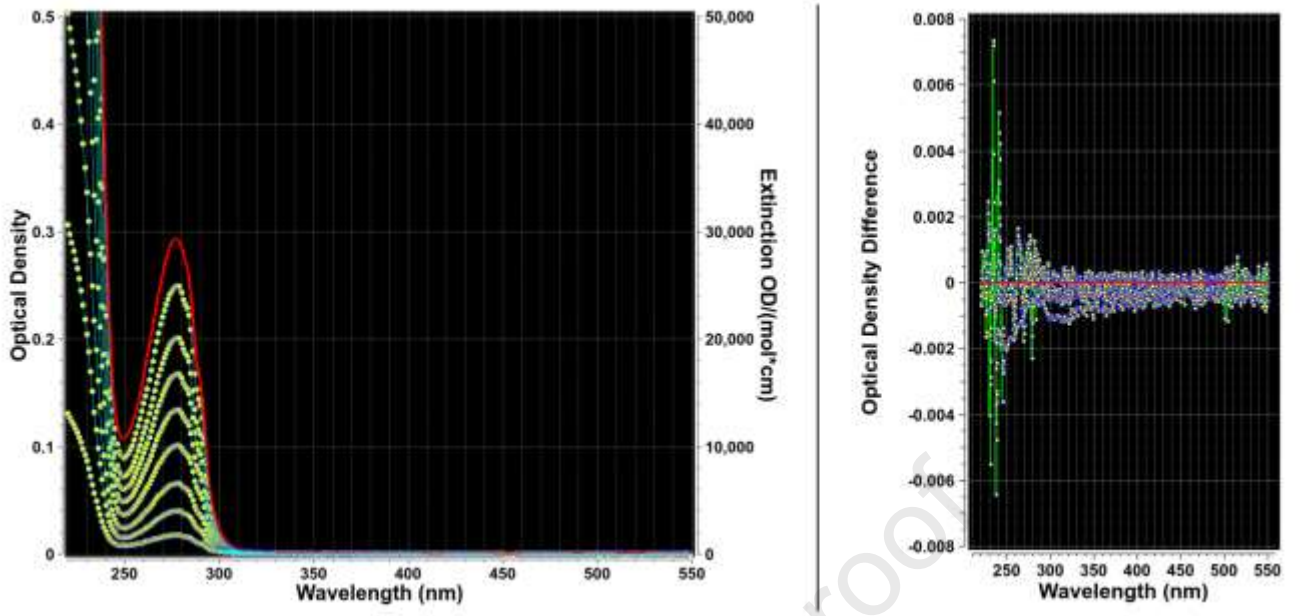

SI 2: Dilution spectra (yellow) and the intrinsic extinction coefficient spectrum (red) of nanobody (left). Residuals of the global nonlinear least squares extinction profile fitting with a standard deviation of 6.30e-4 (right).

Supplemental Figures

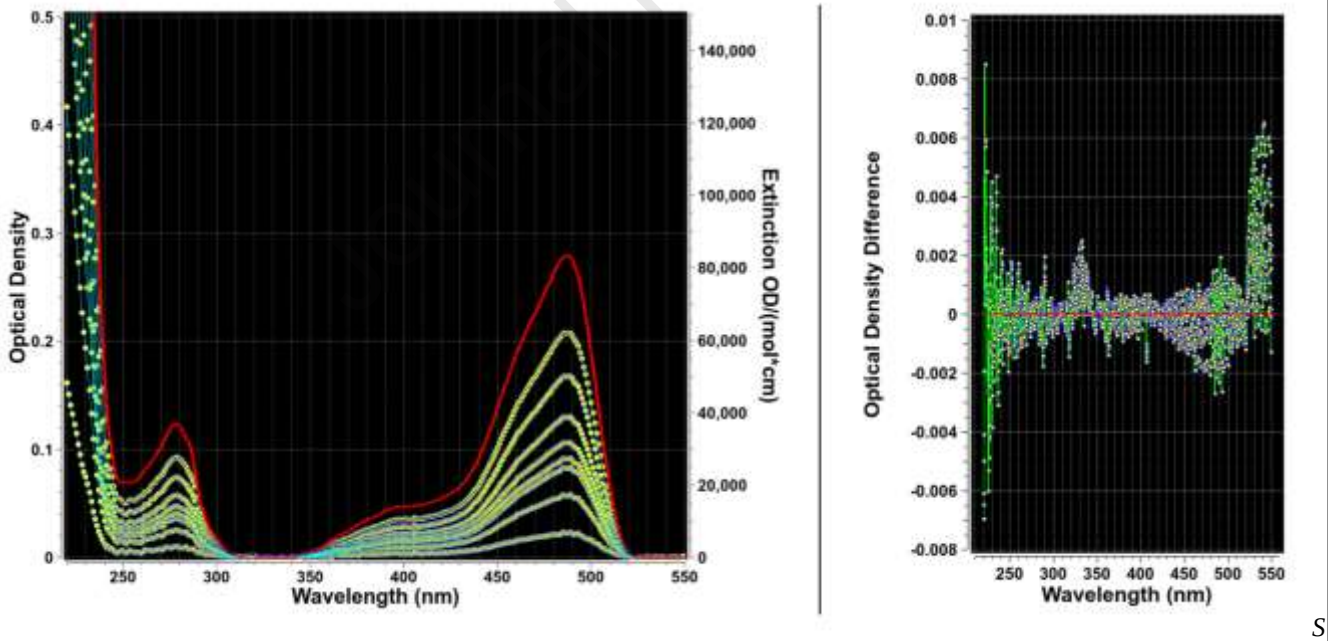

SI 1: Dilution spectra (yellow) and the intrinsic extinction coefficient spectrum (red) of sfGFP (left). Residuals of the global nonlinear least squares extinction profile fitting with a variance of 1.40e-6 and a standard deviation of 1.18e-3 (right).

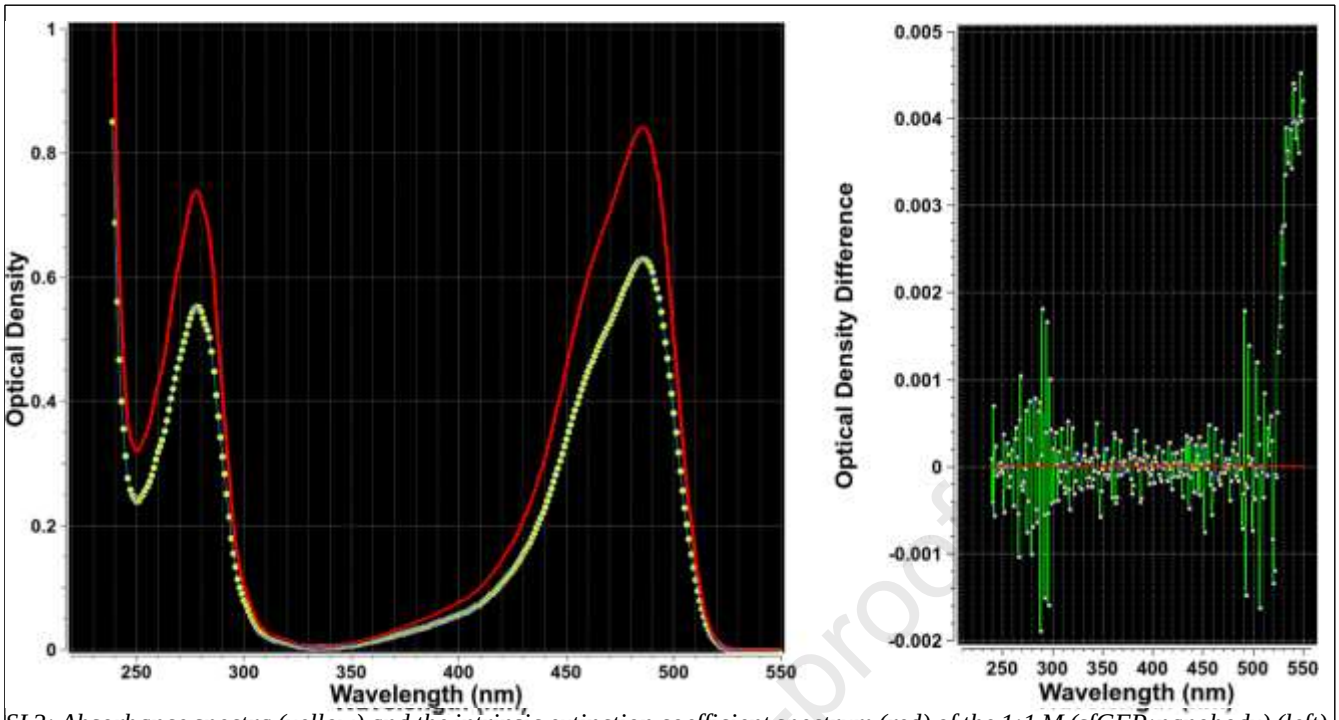

SI 3: Absorbance spectra (yellow) and the intrinsic extinction coefficient spectrum (red) of the 1:1 M (sfGFP:nanobody) (left). SI 4: Absorbance spectra (yellow) and the intrinsic extinction coefficient spectrum (red) of the 1:2 M (sfGFP:nanobody) (left). Residuals of the global nonlinear least squares extinction profile fitting with a variance of 3.58e-6 and a standard deviation of 1.89e-3 (right).

References:

[1]Kirchhofer A, Helma J, Schmidthals K, Frauer C, Cui S, Karcher A, Pellis M, Muyldermans S, Casas-Delucchi CS, Cardoso MC, Leonhardt H, Hopfner KP, Rothbauer U. Modulation of protein properties in living cells using nanobodies. Nat Struct Mol Biol. 2010 Jan;17(1):133-8. doi: 10.1038/nsmb.1727. Epub 2009 Dec 13. PMID: 20010839.

[2]Zhang Z, Wang Y, Ding Y, Hattori M. Structure-based engineering of anti-GFP nanobody tandems as ultra-high-affinity reagents for purification. Sci Rep. 2020 Apr 10;10(1):6239. doi: 10.1038/s41598-020-62606-7. PMID: 32277083; PMCID: PMC7148334.

[3]Yu YA, Szalay AA, Wang G, Oberg K. Visualization of molecular and cellular events with green fluorescent proteins in developing embryos: a review. Luminescence. 2003 Jan-Feb;18(1):1-18. doi: 10.1002/bio.701. Erratum in: Luminescence. 2003 Jul-Aug;18(4):243. PMID: 12536374.

[4]Misteli T, Spector DL. Applications of the green fluorescent protein in cell biology and biotechnology. Nat Biotechnol. 1997 Oct;15(10):961-4. doi: 10.1038/nbt1097-961. PMID: 9335045.

[5]Pédelacq JD, Cabantous S, Tran T, Terwilliger TC, Waldo GS. Engineering and characterization of a superfolder green fluorescent protein. Nat Biotechnol. 2006 Jan;24(1):79-88. doi: 10.1038/nbt1172. Epub 2005 Dec 20. Erratum in: Nat Biotechnol. 2006 Sep;24(9):1170. PMID: 16369541.

[6]Weinstein JY, Martí-Gómez C, Lipsh-Sokolik R, Hoch SY, Liebermann D, Nevo R, Weissman H, Petrovich-Kopitman E, Margulies D, Ivankov D, McCandlish DM, Fleishman SJ. Designed active-site library reveals thousands of functional GFP variants. Nat Commun. 2023 May 20;14(1):2890. doi: 10.1038/s41467-023-38099-z. PMID: 37210560; PMCID: PMC10199939.

[7]Stepanenko OV, Verkhusha VV, Kuznetsova IM, Uversky VN, Turoverov KK. Fluorescent proteins as biomarkers and biosensors: throwing color lights on molecular and cellular processes. Curr Protein Pept Sci. 2008 Aug;9(4):338-69. doi: 10.2174/138920308785132668. PMID: 18691124; PMCID: PMC2904242.

[8]Stevens TA, Tomaleri GP, Hazu M, Wei S, Nguyen VN, DeKalb C, Voorhees RM, Pleiner T. A nanobody-based strategy for rapid and scalable purification of human protein complexes. Nat Protoc. 2024 Jan;19(1):127-158. doi: 10.1038/s41596-023-00904-w. Epub 2023 Nov 16. PMID: 37974029.

[9]Cong ATQ, Witter TL, Schellenberg MJ. High-efficiency recombinant protein purification using mCherry and YFP nanobody affinity matrices. Protein Sci. 2022 Sep;31(9):e4383. doi: 10.1002/pro.4383. PMID: 36040252; PMCID: PMC9413470.

[10]Gill SC, von Hippel PH. Calculation of protein extinction coefficients from amino acid sequence data. Anal Biochem. 1989 Nov 1;182(2):319-26. doi: 10.1016/0003-2697(89)90602-7. Erratum in: Anal Biochem 1990 Sep;189(2):283. PMID: 2610349.

[11]Demeler B., Gorbet G.E. (2016) Analytical Ultracentrifugation Data Analysis with UltraScan-III. In: Uchiyama S., Arisaka F., Stafford W., Laue T. (eds) Analytical Ultracentrifugation. Springer, Tokyo. https://doi.org/10.1007/978-4-431-55985-6_8

[12]Philo JS. SEDNTERP: a calculation and database utility to aid interpretation of analytical ultracentrifugation and light scattering data. Eur Biophys J. 2023 Jul;52(4-5):233-266. doi: 10.1007/s00249-023-01629-0. Epub 2023 Feb 15. PMID: 36792822.

[13]Hoffmann A, Grassl K, Gommert J, Schlesak C, Bepperling A. Precise determination of protein extinction coefficients under native and denaturing conditions using SV-AUC. Eur Biophys J. 2018 Oct;47(7):761-768. doi: 10.1007/s00249-018-1299-x. Epub 2018 Apr 17. PMID: 29666888.

[14]Henrickson A, Gorbet GE, Savelyev A, Kim M, Hargreaves J, Schultz SK, Kothe U, Demeler B. Multi-

wavelength analytical ultracentrifugation of biopolymer mixtures and interactions. Anal Biochem. 2022 Sep 1;652:114728. doi: 10.1016/j.ab.2022.114728. Epub 2022 May 21. PMID: 35609686; PMCID: PMC10276540.

[15]Demeler B. Methods for the Design and Analysis of Analytical Ultracentrifugation Experiments. Curr Protoc. 2024 Feb;4(2):e974. doi: 10.1002/cpz1.974. PMID: 38319042; PMCID: PMC10857736.

[16]Wilkins MR, Gasteiger E, Bairoch A, Sanchez JC, Williams KL, Appel RD, Hochstrasser DF. Protein identification and analysis tools in the ExPASy server. Methods Mol Biol. 1999;112:531-52. doi: 10.1385/1-59259-584-7:531. PMID: 10027275.

[17]Jerabek-Willemsen M, Wienken CJ, Braun D, Baaske P, Duhr S. Molecular interaction studies using microscale thermophoresis. Assay Drug Dev Technol. 2011 Aug;9(4):342-53. doi: 10.1089/adt.2011.0380. PMID: 21812660; PMCID: PMC3148787.

[18]Saponaro A. Isothermal Titration Calorimetry: A Biophysical Method to Characterize the Interaction between Label-free Biomolecules in Solution. Bio Protoc. 2018 Aug 5;8(15):e2957. doi: 10.21769/BioProtoc.2957. PMID: 34395765; PMCID: PMC8328675.

[19]Gorbet GE, Pearson JZ, Demeler AK, Cölfen H, Demeler B. Next-Generation AUC: Analysis of Multiwavelength Analytical Ultracentrifugation Data. Methods Enzymol. 2015;562:27-47. doi: 10.1016/bs.mie.2015.04.013. Epub 2015 Aug 21. PMID: 26412646.

[20]Durchschlag, H. (1986) Specific Volumes of biological macromolecules and some other molecules of biological interest. Thermodynamic Data for Biochemistry and Biotechnology. 45-128. Edited by H.-J. Hinz, Berlin, Springer Verlag.

[21]Cohn, E. J., and Edsall, J. T. (1943) Proteins, Amino Acids, and Peptides as Ions and Dipolar Ions. New York, Reinhold.

[22]Demeler B. Measuring molecular interactions in solution using multi-wavelength analytical ultracentrifugation: combining spectral analysis with hydrodynamics. Biochem (Lond). 2019;41(2):14-18. doi: 10.1042/bio04102014. Epub 2019 Apr 1. PMID: 32952314; PMCID: PMC7500494.

[23]Mortezazadeh S, Demeler B. A spectral decomposition quality assessment tool for multi-wavelength AUC experiments with UltraScan. Eur Biophys J. 2023 Jul;52(4-5):303-310. doi: 10.1007/s00249-023-01640-5. Epub 2023 Mar 17. PMID: 36930298; PMCID: PMC10505247.

[24]Stoutjesdyk M, Henrickson A, Minors G, Demeler B. A calibration disk for the correction of radial errors from chromatic aberration and rotor stretch in the Optima AUC™ analytical ultracentrifuge. Eur Biophys J. 2020 Dec;49(8):701-709. doi: 10.1007/s00249-020-01434-z. Epub 2020 May 9. PMID: 32388675.

[25]Brookes E, Cao W, Demeler B. A two-dimensional spectrum analysis for sedimentation velocity experiments of mixtures with heterogeneity in molecular weight and shape. Eur Biophys J. 2010 Feb;39(3):405-14. doi: 10.1007/s00249-009-0413-5. Epub 2009 Feb 27. PMID: 19247646.

[26]Demeler B and E. Brookes. Monte Carlo analysis of sedimentation experiments. Colloid Polym Sci (2008) 286(2) 129-137

[27]Demeler B, van Holde KE. Sedimentation velocity analysis of highly heterogeneous systems. Anal Biochem. 2004 Dec 15;335(2):279-88. doi: 10.1016/j.ab.2004.08.039. PMID: 15556567.

[28]MacGregor IK, Anderson AL, Laue TM. Fluorescence detection for the XLI analytical ultracentrifuge. Biophys Chem. 2004 Mar 1;108(1-3):165-85. doi: 10.1016/j.bpc.2003.10.018. PMID: 15043928.

[29]Yu L, Lei Y, Ma Y, Liu M, Zheng J, Dan D, Gao P. A Comprehensive Review of Fluorescence Correlation Spectroscopy. Front. Phys. 2021 9:644450. doi: 10.3389/fphy.2021.644450.

[30]Steele HBB, Elmer-Dixon MM, Rogan JT, Ross JBA, Bowler BE. The Human Cytochrome *c* Domain-Swapped Dimer Facilitates Tight Regulation of Intrinsic Apoptosis. Biochemistry. 2020 Jun 9;59(22):2055-2068. doi: 10.1021/acs.biochem.0c00326. Epub 2020 Jun 1. PMID: 32428404; PMCID: PMC7291863.

[31]Petrásek Z, Schwille P. Precise measurement of diffusion coefficients using scanning fluorescence

correlation spectroscopy. Biophys J. 2008 Feb 15;94(4):1437-48. doi: 10.1529/biophysj.107.108811. Epub 2007 Oct 12. PMID: 17933881; PMCID: PMC2212689.

[32]Wyatt, P. J. (1993). Light scattering and the absolute characterization of macromolecules. Analytica Chimica Acta, 272(1), 1–40. doi:10.1016/0003-2670(93)80373-s

[33]Stetefeld J, McKenna SA, Patel TR. Dynamic light scattering: a practical guide and applications in biomedical sciences. Biophys Rev. 2016 Dec;8(4):409-427. doi: 10.1007/s12551-016-0218-6. Epub 2016 Oct 6. PMID: 28510011; PMCID: PMC5425802.

[34]D.P. Buser, K.D. Schleicher, C. Prescianotto-Baschong, M. Spiess, A versatile nanobody-based toolkit to analyze retrograde transport from the cell surface, Proc. Natl. Acad. Sci. U.S.A.115 (27) E6227-E6236, https://doi.org/10.1073/pnas.1801865115 (2018).

[35]Shilling PJ, Mirzadeh K, Cumming AJ, Widesheim M, Köck Z, Daley DO. Improved designs for pET expression plasmids increase protein production yield in Escherichia coli. Commun Biol. 2020 May 7;3(1):214. doi: 10.1038/s42003-020-0939-8. PMID: 32382055; PMCID: PMC7205610.

[36]Kubala MH, Kovtun O, Alexandrov K, Collins BM. Structural and thermodynamic analysis of the GFP:GFP-nanobody complex. Protein Sci. 2010 Dec;19(12):2389-401. doi: 10.1002/pro.519. PMID: 20945358; PMCID: PMC3009406.

[37]Kirchhofer A, Helma J, Schmidthals K, Frauer C, Cui S, Karcher A, Pellis M, Muyldermans S, Casas-Delucchi CS, Cardoso MC, Leonhardt H, Hopfner KP, Rothbauer U. Modulation of protein properties in living cells using nanobodies. Nat Struct Mol Biol. 2010 Jan;17(1):133-8. doi: 10.1038/nsmb.1727. Epub 2009 Dec 13. PMID: 20010839.

[38]Gura Sadovsky R, Brielle S, Kaganovich D, England JL. Measurement of Rapid Protein Diffusion in the Cytoplasm by Photo-Converted Intensity Profile Expansion. Cell Rep. 2017 Mar 14;18(11):2795-2806. doi: 10.1016/j.celrep.2017.02.063. PMID: 28297680; PMCID: PMC5368347.

[39]Mullineaux CW, Nenninger A, Ray N, Robinson C. Diffusion of green fluorescent protein in three cell environments in Escherichia coli. J Bacteriol. 2006 May;188(10):3442-8. doi: 10.1128/JB.188.10.3442-3448.2006. PMID: 16672597; PMCID: PMC1482841.

[40]Terry BR, Matthews EK, Haseloff J. Molecular characterisation of recombinant green fluorescent protein by fluorescence correlation microscopy. Biochem Biophys Res Commun. 1995 Dec 5;217(1):21-7. doi: 10.1006/bbrc.1995.2740. PMID: 8526912.

[41]Swaminathan R, Hoang CP, Verkman AS. Photobleaching recovery and anisotropy decay of green fluorescent protein GFP-S65T in solution and cells: cytoplasmic viscosity probed by green fluorescent protein translational and rotational diffusion. Biophys J. 1997 Apr;72(4):1900-7. doi: 10.1016/S0006-3495(97)78835-0. PMID: 9083693; PMCID: PMC1184383.

[42]Busch NA, Kim T, Bloomfield VA. Tracer Diffusion of Proteins in DNA Solutions. 2. Green Fluorescent Protein in Crowded DNA Solutions. Macromolecules 2000 33 (16), 5932-5937 DOI: 10.1021/ma0005724

[43]Visser, A.J.W.G., Hink, M.A. New Perspectives of Fluorescence Correlation Spectroscopy. Journal of Fluorescence 9, 81–87 (1999).

[44]Zhao H, Schuck P. Global multi-method analysis of affinities and cooperativity in complex systems of macromolecular interactions. Anal Chem. 2012 Nov 6;84(21):9513-9. doi: 10.1021/ac302357w. Epub 2012 Oct 16. PMID: 23020071; PMCID: PMC3491091.

- Dynamic interactions between biopolymers can be effectively studied in the solution phase
- Results available from MW-AUC, SEC-MALS, SEC-DLS are in very good agreement
- Dynamic range, signal-to-noise ratio, sensitivity are complemented by multiple techniques
- ITC, MST, and fluorescence AUC perform best in measuring thermodynamics in the nanomolar range.
- MW-AUC excels at defining stoichiometry and composition
- MW-AUC, SEC-DLS, and FCS provide similar diffusion coefficients

Authors

Aysha K. Demeler[1*)], James Bosco[2*)], Matthew J. Sydor[2,3], Michelle Nemetchek[2,3], Saeed Mortezazadeh[1], Liam Kerr[1], Sophia Bird[1], Roza Gabdullina[1], Cindee Yates-Hansen[3], Levi J. McClelland[2,3], Ekaterina Voronina[3], Trushar R. Patel[1], Borries Demeler[1,2**)]

*) Equal contribution

**) Corresponding Author

1. Department of Chemistry and Biochemistry, University of Lethbridge, Lethbridge, AB, T1K 3M4, Canada

2. Department of Chemistry and Biochemistry, University of Montana, Missoula, MT 59812, USA

3. Division of Biological Sciences, University of Montana, Missoula, MT 59812, USA

4. Center for Biomolecular Structure & Dynamics, University of Montana, Missoula, MT 59812, USA

Declaration of Interest Statement

☒ The authors declare that they have no known competing financial interests or personal relationships that could have appeared to influence the work reported in this paper.

☐ The author is an Editorial Board Member/Editor-in-Chief/Associate Editor/Guest Editor for this journal and was not involved in the editorial review or the decision to publish this article.

☐ The authors declare the following financial interests/personal relationships which may be considered as potential competing interests: